

6 Transport in an n-channel Strained Silicon Device

6.1 Abstract

Previous chapters have stressed the importance of silicon-germanium in terms of improving the mobility of holes in semiconductor materials. However, it is also important to study the characteristics of electron gases in strained silicon-germanium heterostructures if both n- and p-channel devices are to be integrated. The physics of 2-dimensional electronic systems is also simpler and more fully understood in some respects than it is for holes. Additionally, the mobility of electrons is generally better than that of holes, in a given system, so transport in a more metallic regime can be investigated and classical magnetoresistance is more easily analyzed.

6.2 Introduction

Pure, unstrained silicon has 6 conduction band minima. Tensile strain (perpendicular to the growth direction, as occurs when pure silicon is grown on relaxed silicon-germanium alloy) causes the two minima in the growth direction to lie at a lower energy than the four minima in the plane. This greatly reduces intervalley scattering.¹

Since the structure of the device (Figure 6.1) is "normal" the heterointerface at which the 2DEG is defined should be of high quality, the electron channel should have a high mobility.² Quantum effects which rely on disorder and impurities (for example, weak localization) should not visibly influence the transport.

6.3 Structure

The structure of the n-channel device is shown in Figure 6.1. It was grown by Gas Source Molecular Beam Epitaxy at Imperial College, by R. Ferguson. The dopant layer is above the active channel making this a "normal" structure and so there is no gate and the electron concentration is not variable.

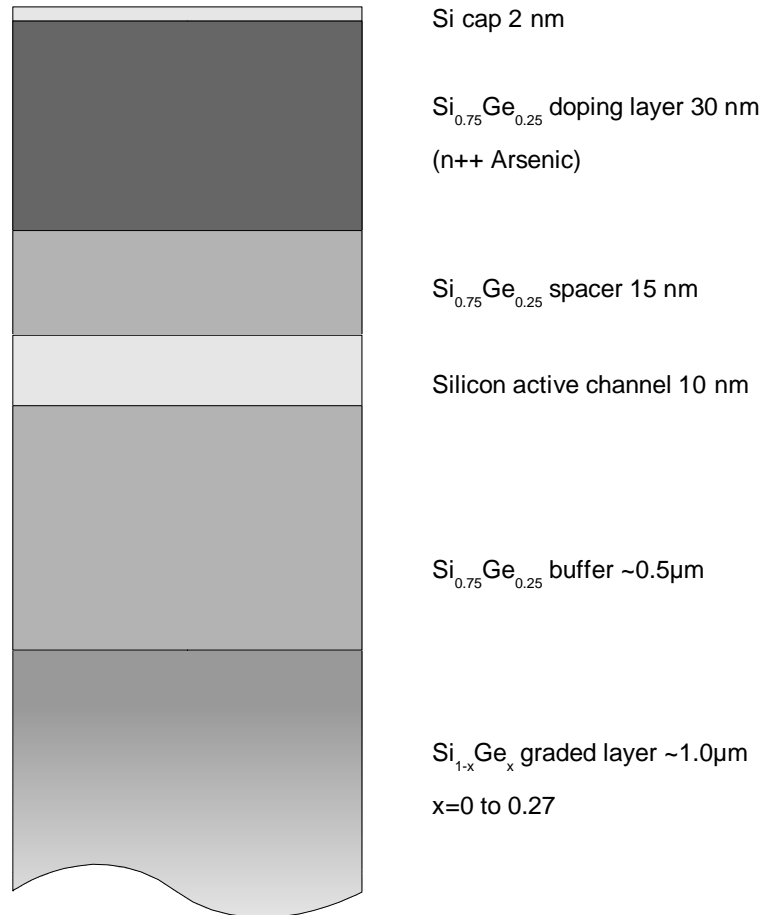


Figure 6.1 The structure of the n-type device. There is a thick, graded layer followed by an alloy buffer layer. There is heavy n-type doping above the active channel and there is no gate.

The active channel of pure silicon was grown on a "virtual substrate" of relaxed $\text{Si}_{0.75}\text{Ge}_{0.25}$ and capped by the same material, causing it to be under tensile strain and creating a quantum well for electrons. (This is in contrast with the p-channel devices considered in Chapters 5 and 7, in which the active $\text{Si}_{1-x}\text{Ge}_x$ channels are pseudomorphically grown on pure silicon leading them to compressively strained, forming quantum wells for holes.)

Calculations for this heterostructure yield a band gap in the active channel of 0.90eV (compared to 1.17eV for unstrained silicon or 1.09eV for the unstrained $\text{Si}_{0.75}\text{Ge}_{0.25}$ alloy) and an effective mass for the electrons in the two Δ out-of-plane minima of $0.199m_e$. The conduction band offset between the active channel and its surrounding layers is 250meV and the valence band is 60meV lower in the active channel making this a Type II structure. The splitting between the in-plane and out-of-plane conduction band minima is 200meV. ³

Calculations similar to those described for a p-type system in Equation 3.1 and Figure 3.1 suggest that the sheet carrier concentration of electrons in the active channel (at the upper heterointerface) will be $\sim 10^{12}\text{cm}^{-2}$ at $T \ll T_F$; for this sheet density and effective mass (and taking into account the double valley degeneracy) the Fermi temperature will be $\sim 70\text{K}$.

6.4 Classical Magnetoresistance and Mobility Spectrum Analysis

Data for the variation of resistivity with magnetic field, at various temperatures, are shown in Figures 6.2 to 6.4. Chapter 4 describes both the utility of measurements of magnetoresistance in the classical regime and the problems associated with their interpretation. Equations 4.10 and 4.11 show how elements of the conductivity tensor $\sigma(B)$ can be found in terms of the function $s(\mu)$ (Equation 4.12) through integral transformation. (Equations 4.13 and 4.14 relate $\sigma(B)$ to the more usually measured quantities of the longitudinal resistivity $\rho(B)$ and the Hall coefficient $R_H(B)$.)

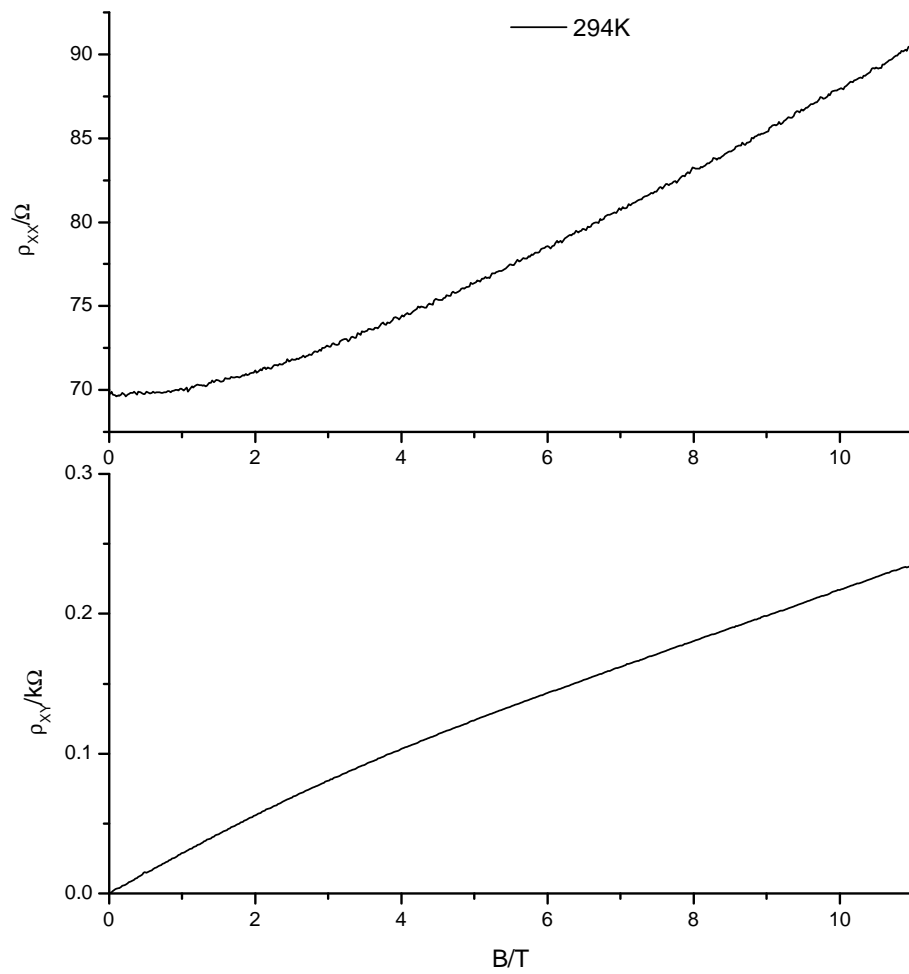


Figure 6.2 Magnetoresistance at 294K. It is clear from the gradient of the ρ_{xy} data that the Hall coefficient is decreasing as magnetic field increases.

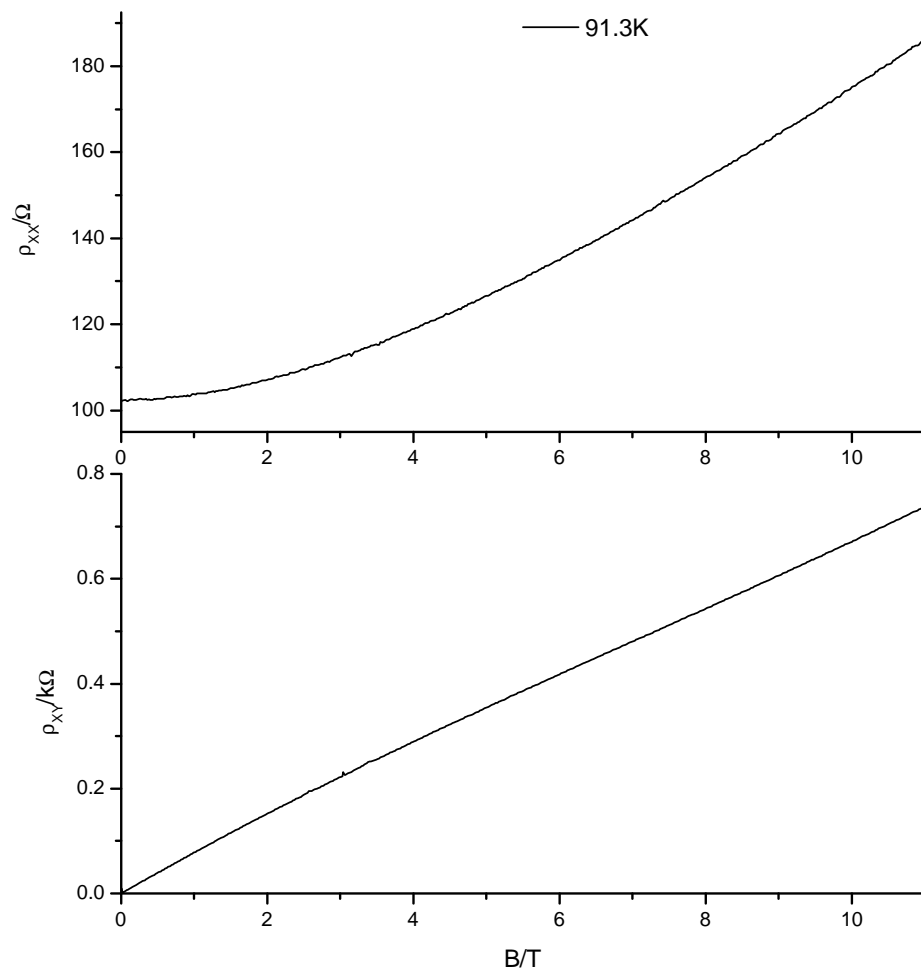


Figure 6.3 Magnetoresistance at 91K. The scales of the vertical axes has changed from Figure 6.2, but the forms of the curves are similar.

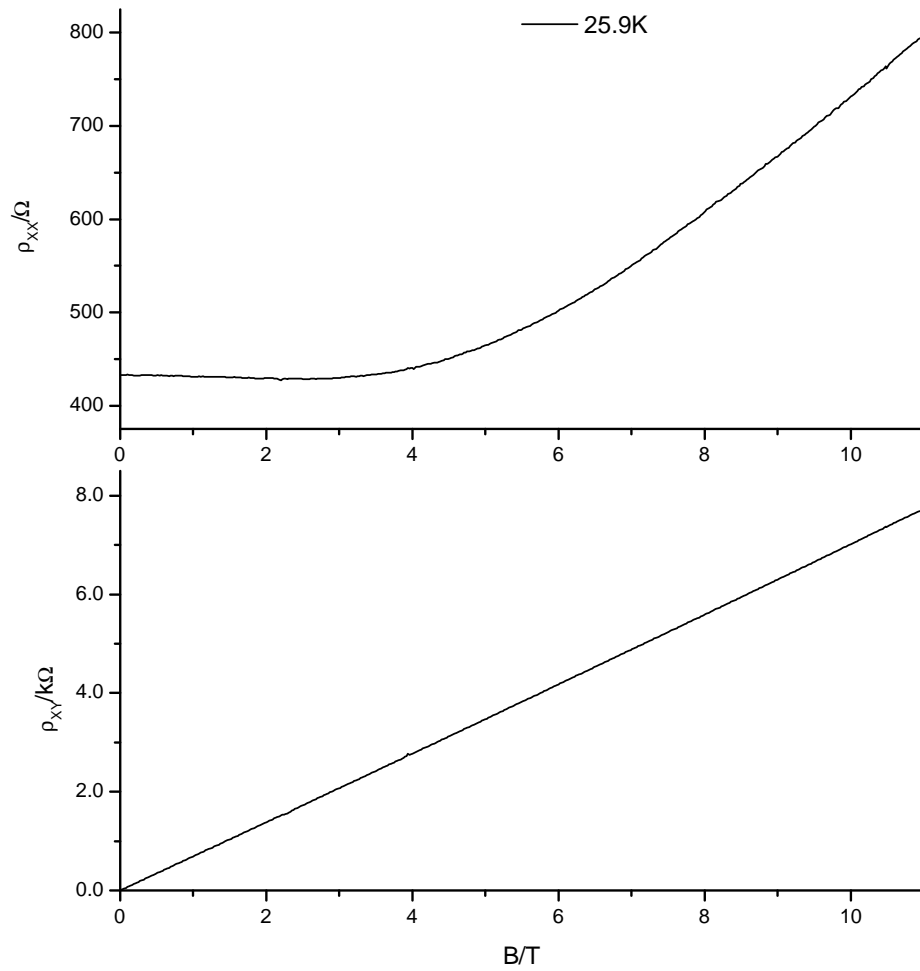


Figure 6.4 Magnetoresistance at 26K. The Hall coefficient is effectively constant with respect to magnetic field. For fields up to 4T, there is little longitudinal magnetoresistance: this corresponds to the limit of $\hbar \omega_C \sim k_B T$. Eventually, as temperature decreases, Shubnikov-de Haas oscillations will appear.

This function $s(\mu)$ is known as the mobility spectrum. This gives the contribution to the conductivity of the system due to carriers with mobility μ . It is assumed in this investigation that this function does not change with magnetic field; this will not be true when $\hbar\omega_c \geq k_B T$ (Landau levels are formed) or when the carriers become weakly localized since both these conditions involve magnetic-field dependent mobility. Under this assumption, magnetoresistance is always positive; negative magnetoresistance can be analyzed using the assumption of a magnetic-field dependence of the mobility.⁴ Significant intersubband scattering can also invalidate this method.⁵

To find the magnetoresistance given a form for the mobility spectrum is straightforward. Finding the mobility spectrum from magnetoresistance data, however, is an inverse transform problem and therefore more difficult and the subject of much investigation.^{6,7,8,9,10,11} Some of these approaches will now be briefly reviewed, before considering the method of maximum entropy in more detail.

(i) Reference 6, which first introduced the concept of the mobility spectrum, involves a mathematically complicated solution method, the numerical details of which will not be explored. The number of data points used to create a solution is equal to the number of distinct carrier gases within the sample, plus one. The solution method may either proceed by searching for an imposed number of carrier gases or be free to start by attempting a fit for a single gas, and then a two-gas system, and so on. For each search for n gases, the method must try each combination of $n+1$ data points from the whole data set, keeping the sets which lead to "physical" solutions, and from these sets generate an "envelope function" within which the mobility spectrum is found.

Once a set of carrier gases has been found, a least-squares fit on the original data is performed with the carrier gas parameters as variables. If this fit is satisfactory and the parameters emerge virtually unscathed then the results of the original analysis can be considered reasonable.

If only a limited number of data points (~ 10) are available and the system is

expected to contain only two or three distinct carrier gases, then this method is quite efficient. However, the data collected in this part of the investigation generally comprises resistivity data at about 500 magnetic field values and the system simply cannot cope; to choose points or create averaged data by hand is to impose artificial constraints on the final solution. Also, this method does not respond well to errors in the experimental data.¹¹

(ii) Reference 7 introduces and describes the Reduced Conductivity Tensor method for extracting the carrier concentration and mobility of each component of a multilayer semiconductor system. Assumptions are made that the carrier gases are essentially degenerate and that the effective mass is isotropic, but nevertheless, agreement between theory and experiment is good.

(iii) In Reference 8, it is assumed that the mobility for a mixed scattering can be approximated by the phenomenological expression:

$$\mu = \mu_0 x^\alpha \quad \text{where} \quad x = \frac{E}{k_B T} \quad 6.1$$

and that the mobility spectrum of non-degenerate carriers in a spherical band can be approximated by:

$$s(\mu) = S_0 e^{-x(\mu)} x(\mu)^{2.5} \quad 6.2$$

where S_0 , μ_0 and α are coefficients depending on the density of states and on the parameters of all the scattering mechanisms. Then, the integration over the whole mobility spectrum in Equations 4.10 and 4.11 is converted to summation of discrete spectra for electrons and holes and an iterative transformation procedure is performed. The results are decomposed into high-mobility carrier and low-mobility carrier contributions, the division chosen arbitrarily, with results for the former seeming much more satisfactory than results for the latter.

(iv) References 9 and 10 describe the "quantitative mobility spectrum technique" (QMSA) and the "improved quantitative mobility spectrum technique" (i-QMSA) respectively. These, again, are iterative techniques but with no initial assumption about the solution (although the method from Reference 6 is used to create the first trial solution to iterate, and conductivity data is extrapolated to higher magnetic field values to extend the available mobility range). The i-QMSA method introduces a few extra tricks for improving the fits whilst smoothing the spectra and making them more physically reasonable.

A serious issue (regarding inverse transformation problems in general) is that while a particular spectrum $s(\mu)$ may, upon the action of an integral transform over the "kernel function" $K(B, \mu)$, produce a magnetoconductivity $\sigma(B)$, the inverse problem is ill-conditioned and the solution obtained for $s(\mu)$ by inverting the kernel is extremely sensitive to small changes or errors in the $\sigma(B)$ data. Also, a particular $s(\mu)$ is not a unique solution, within the uncertainty bounds of the original noisy and incomplete $\sigma(B)$ data.

6.4.1 Maximum Entropy Method of Mobility Spectrum Analysis

The technique of "Maximum Entropy" has been employed to solve this and other problems involving inverse integral transformation where the result is a positive, additive function.^{11,12,13,14} Generally, if two solutions (found by any means) are of equal merit (in terms of, for example, their least-squares fits to the original results) then the solution with the larger entropy is to be favoured, since it is maximally noncommittal with regard to missing (unmeasured) information in the original data.^{11,15} In other words, the solution favoured by the maximum entropy method extracts the most information out of the original data without making unreasonable assumptions about information which is unavailable.

This method embodies Bayes' theorem: the probability of a particular hypothesis given some data (and any background assumptions) is proportional to the probability of that data given the hypothesis and the assumptions and the probability of

the hypothesis given the assumptions alone.¹²

The entropy S of a discrete mobility spectrum $\{s\}$ can be defined as:¹¹

$$S\{s_j\} = -\sum_{j=1}^n p_j \ln p_j \quad 6.3$$

$$p_j = \frac{s_j}{\sigma_0} \quad 6.4$$

where p_j is the probability of s_j and σ_0 is the conductivity at zero magnetic field. This imposes the condition that the mobility spectrum is non-negative and normalizable, which is physically realistic. However, if any prior information about the form of the spectrum is available then this may be incorporated as a so-called default model $\{m\}$:^{13,14}

$$S(s) = -\sum_{j=1}^n p_j \ln [p_j / m_j] \quad 6.5$$

Fitting is now a matter of minimizing the function Q :¹⁴

$$Q = \chi^2 - \alpha S \quad 6.6$$

where $\chi^2 = \sum_i (\sigma(B_i) - \sigma_c(B_i))^2 / \delta_i^2$; $\sigma_c(B)$ is magnetoconductivity calculated from the fitting mobility spectrum, δ^2 gives a measure of the error in the data (this parameter is conventionally referred to as σ^2 but here is renamed to avoid confusion with conductivity) and α is a hyper-parameter which controls the relative importance of the least-squares and entropic constraints.¹⁴ Full technical details are given in Reference 13 and Chapter 5 of Reference 14. Equation 6.6 can be meaningfully compared to the free energy, $F = E - TS$, which is often to be minimised to find the solution in thermodynamic or statistical-mechanic systems.¹⁸

There are various flavours of the maximum entropy method, which differ in the way in which they approach the hyper-parameter α . In the case of Historic maximum entropy, α is set so that at the minimum of Q (Equation 6.6) $\chi^2 = M$ where M is the number of "observations" or data points. In the case of Classic maximum entropy, the most probable value of α is found, given the data and the default model.^{16,17} Alternatively, the method described in Reference 18 does not use Bayesian inference but treats the maximization of the entropy as a natural starting-point for derivations of other results of statistical mechanics.

The approach of Bryan's algorithm is to calculate solutions for a range of α values and evaluate the probability of each being correct given the data and the default model. These solutions are then averaged, weighted by their probabilities.¹⁴ However, this method does not work very well if α is very small: in the method developed in Reference 14 a solution produced by Bryan's algorithm maximum entropy is used as the default model for the next solution. This procedure is repeated until the the most probable solution corresponds to an α value well within the range of applicability of Bryan's algorithm.

Since the integral transform from $s(\mu)$ to $\sigma(B)$ actually involves two integral equations (Equations 4.11 and 4.12) then we work with¹¹

$$\sigma(B) = \sigma_{XX}(B) + \sigma_{XY}(B) = \int_{-\infty}^{+\infty} \frac{1 + \mu B}{1 + \mu^2 B^2} s(\mu) d\mu \quad 6.7$$

and since the forms for $s(\mu)$ and $\sigma(B)$ are discrete, then Equation 6.7 can be rewritten $\sigma_i = K_{ij} s_j$. The mobility spectrum may be computed as:

$$s_j = K_{ji}^{-1} \sigma_i \quad 6.8$$

Since the magnetoconductivity $\sigma(B_i)$ is relatively insensitive to the details of the

mobility spectrum $s(\mu_j)$ then the kernel contains a large amount of repeated information; many of the linear equations described by the kernel will be (almost) identical.¹⁴ In addition, elements of the kernel matrix which are dominated by small signal noise or computational rounding errors will invert to very large values which will be overpowering in Equation 6.8. If the kernel is an $M \times N$ matrix written as $\mathbf{K} = \mathbf{U} \mathbf{W} \mathbf{V}^T$ with \mathbf{U} an $M \times N$ column-orthogonal matrix, \mathbf{W} as an $N \times N$ diagonal matrix with nonnegative values (the "singular values") and \mathbf{V}^T the transpose of an orthogonal $N \times N$ matrix \mathbf{V} , then the inverse of the kernel can be written as $\mathbf{K}^{-1} = \mathbf{V} \mathbf{W}^{-1} \mathbf{U}^T$.¹⁸

If one of the elements of \mathbf{W} is zero then the corresponding element of \mathbf{W}^{-1} will be infinite and the matrix will be singular. However, by invoking the concepts of *nullspace* and *range* for singular matrices an element of \mathbf{W}^{-1} is set to zero if the corresponding element of \mathbf{W} is zero (or smaller than some set noise floor). This technique of *singular value decomposition* effectively reduces the dimension of the space that must be searched for a solution and discards noise which would corrupt the solution. It is therefore a very important feature of the following analysis. A widely available algorithm for performing singular value decomposition in the C programming language is `svdcmp`, from Numerical Recipes.¹⁸

A simple, powerful and successful maximum-entropy method for finding a mobility spectrum is described in Reference 11, based on the method of Reference 15. The described procedure does not, however, use singular value decomposition to remove overspecification and noise and so the calculation time increases with the square of the product of the number of mobility and magnetic field points, $(NM)^2$; nor does it make explicit a hyper-parameter (α in Equation 6.6) which controls the relative importance of a result which fits the original data versus a result with the maximum the entropy or deal with error in the data in an obvious way.

In the Bryan' sAlgorithm Mobility Spectrum method described below, the calculation time scales as $N^n M$ where n falls from unity to around 0.7 as N increases.

This is a direct result of the singular value decomposition; the time to perform this scales as N^2M but tests and calculations suggest that the number of input points would have to exceed tens of thousands before the SVD was taking as long to perform as the actual maximum entropy inversion. For input data at 500 magnetic field values, and an output spectrum of 1000 points, the BAMS result is produced in 7 hours on a Solaris 360MHz Ultra SPARC-III or 3 hours on a 450MHz Pentium III running Linux.

6.4.2 "Bryan's Algorithm Mobility Spectrum" Results

In Chapter 5 of Reference 14, the techniques of singular value decomposition and iterated Bryan' algorithm maximum entropy are employed to extract a spectral function (related to the density of states) from a static correlation function. The computer code used to perform this task was written by J. P. Hague and then modified in collaboration with the Author to extract a mobility spectrum from magnetoconductivity data.

Mobility spectra produced by application of this method are shown in Figures 6.5, 6.6 and 6.7. Summaries of the mobilities and sheet densities found from these spectra are shown in Figures 6.8 and 6.9 along with values obtained by simple application of Equations 4.7 and 4.9 at low ($\pm 0.5T$) and high ($\pm 10T$) magnetic fields. The manner in which these results have been extracted from the spectra will be explained in the following section. Results for 4.5K, 1.5K and 0.35K are not shown; the 4.5K result is discussed below, the 1.5K and 0.35K result agree on a mobility of $23,000\text{cm}^2\text{V}^{-1}\text{s}^{-1}$ at a sheet density of $9.0 \times 10^{11}\text{cm}^{-2}$.

Figure 6.10 shows how the 2DEG and dopant layer contribute to the overall resistivity of the device, as a function of temperature. It can be seen that, since the resistivity of the dopant layer is several times larger than that of the the 2DEG, it makes little contribution even at high temperatures. The temperature dependence of the resistivity of the 2DEG is the subject of section 6.4.

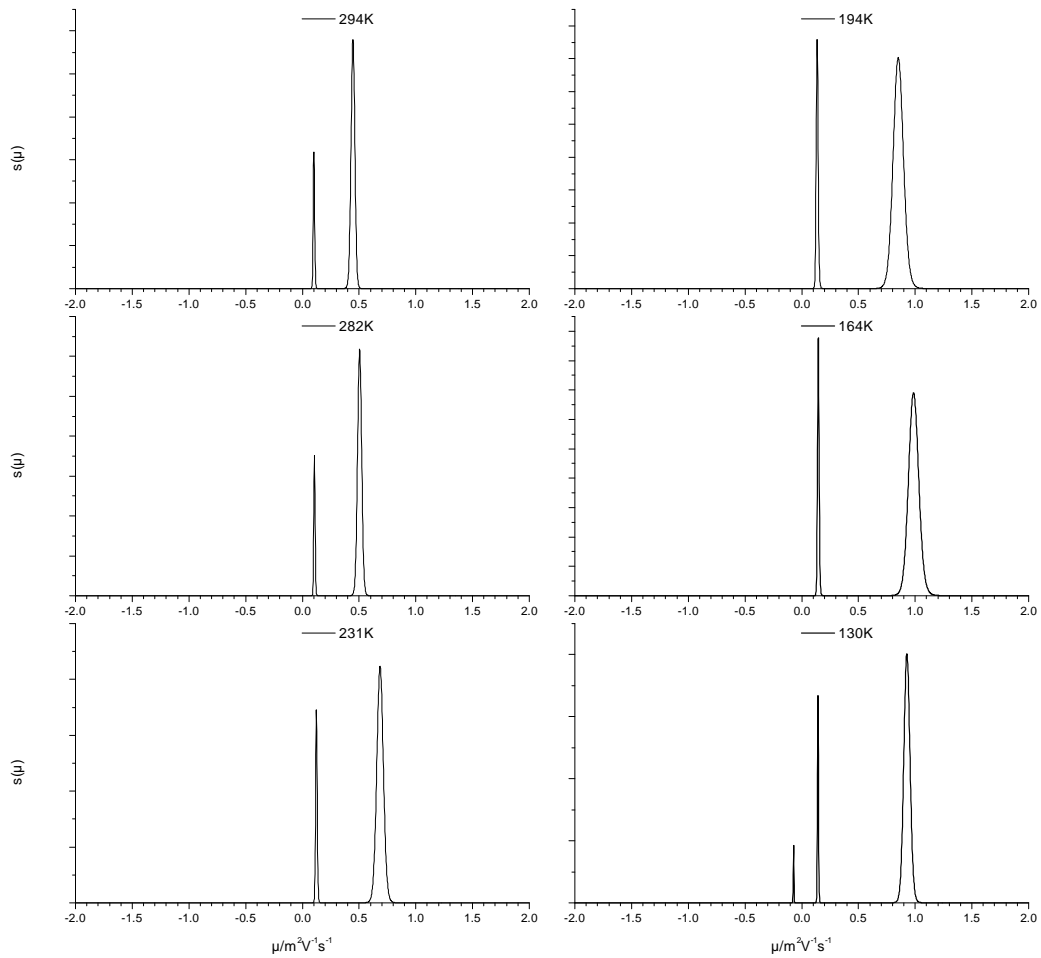


Figure 6.5 Mobility spectrum results produced using maximum entropy analysis. The temperature is shown on each plot. In five of the spectra there are two peaks; the lower mobility peak is ascribed to conduction in the arsenic dopant slab, the higher mobility peak to the 2-dimensional electron gas itself, in the strained silicon active channel. The mobility of the 2DEG peak generally increases as temperature decreases. The third peak in the 130K results will be discussed in the text. The vertical scale in each case is irrelevant: it is the area under each peak that is of importance, not their heights.

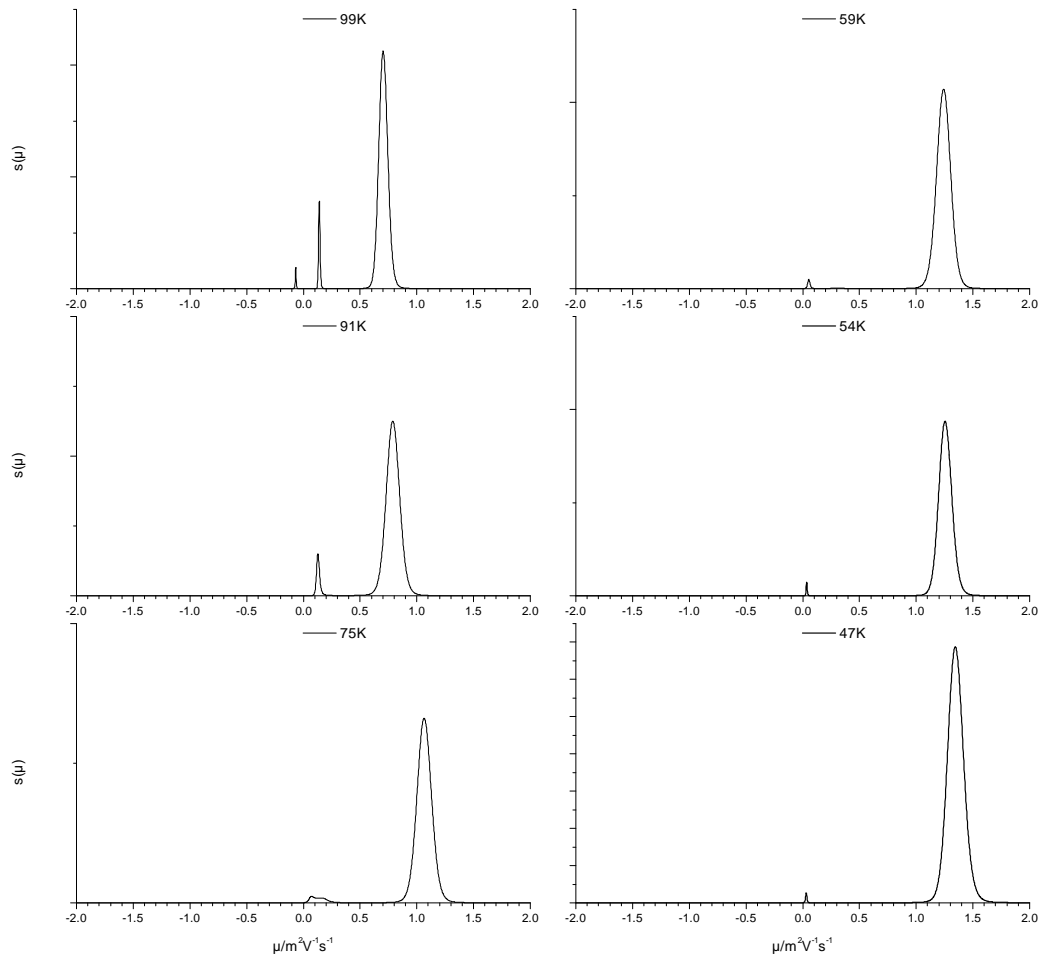


Figure 6.6 (continuation from Figure 6.5) As temperature decreases further, the mobility of the 2DEG peak continues to increase while the dopant slab peak diminishes.

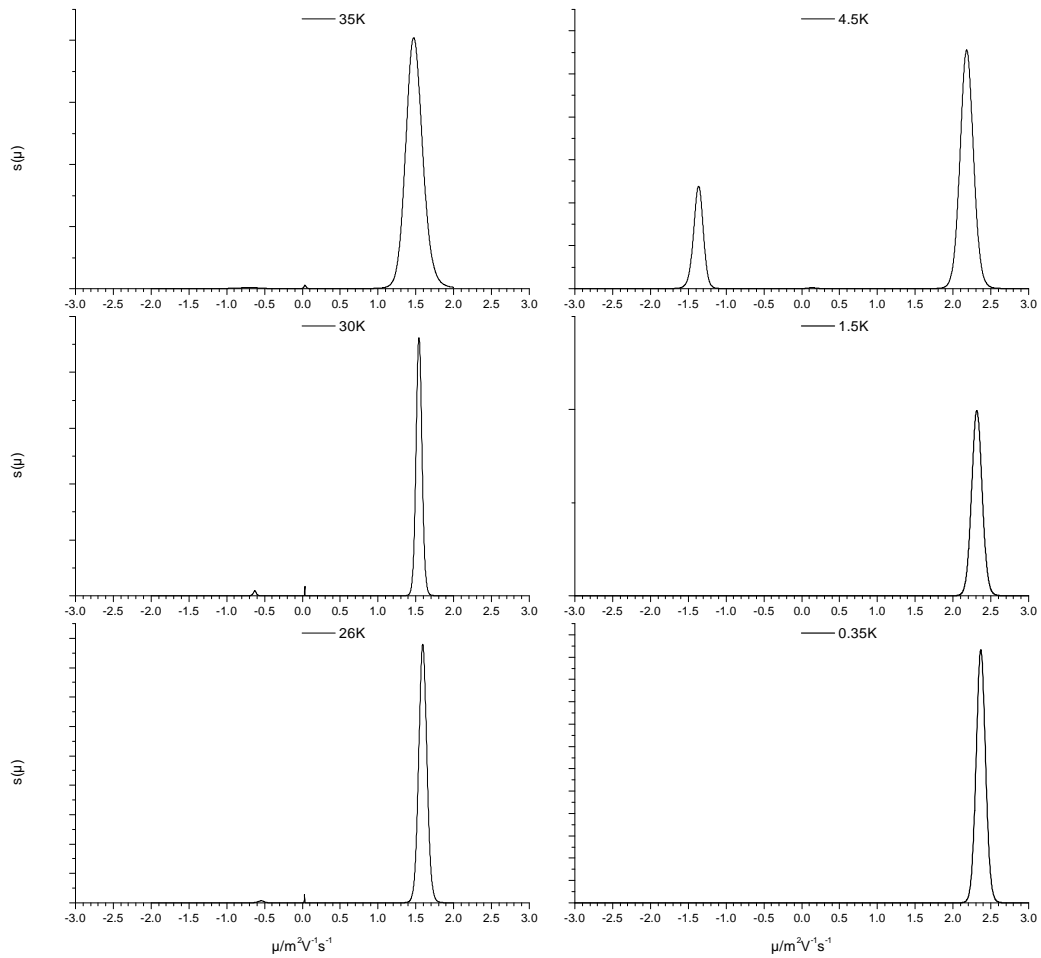


Figure 6.7 (continuation from Figure 6.6 but with an extended x-axis scale) The 2DEG peak reaches a high mobility, and only faint vestiges and artifacts remain in the rest of the spectrum. The exception is the 4.5K result, which features a significant peak in the "negative mobility" region. If this were genuine (see text) it would signify high-quality p-type conduction. Data used for these low-temperature results were limited to lower magnetic fields so as to avoid the Shubnikov-de Haas regime.

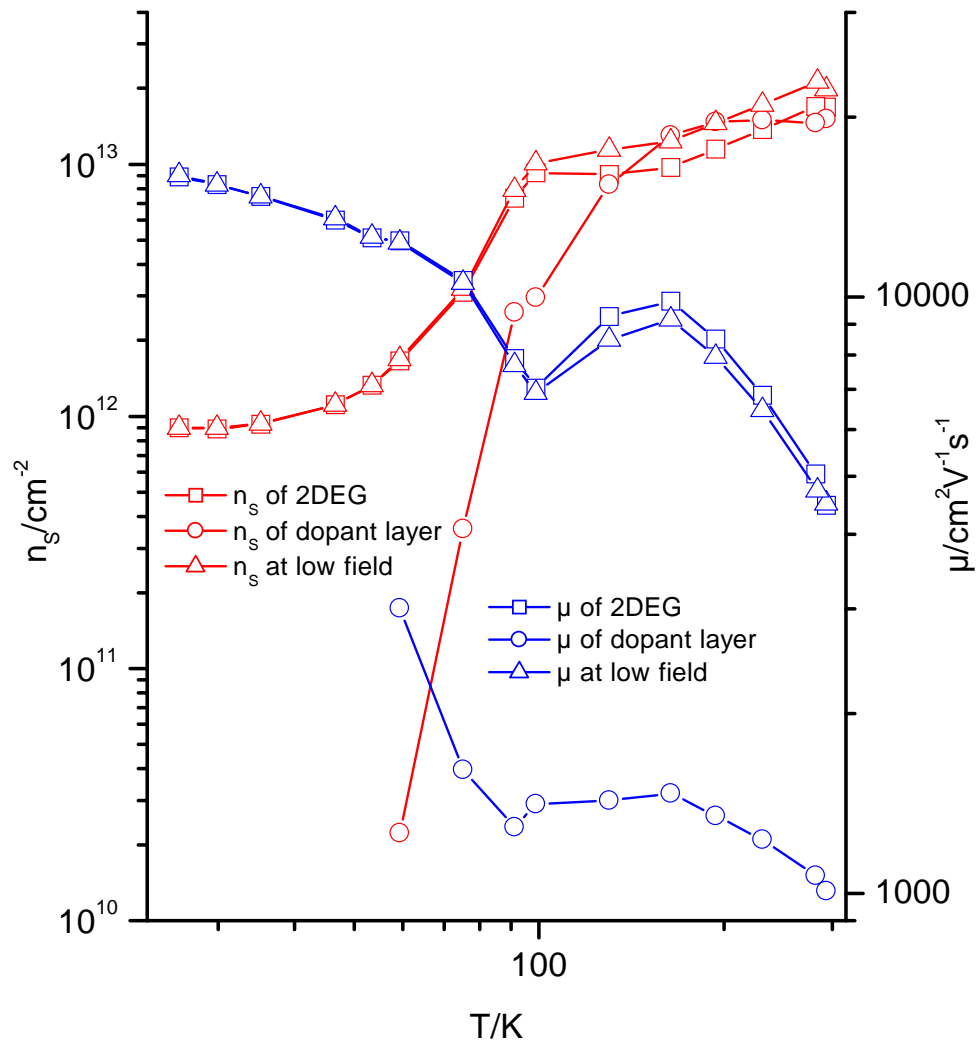


Figure 6.8 A summary of results extracted from magnetoresistance measurements. The mobilities of the two main peaks in the spectra are shown (ascribed to the 2DEG and the dopant) as are the effective sheet densities obtained by their integration. Mobilities and sheet densities measured directly using assumption of the single-carrier Hall effect at low magnetic field are also shown. At low temperatures, the low-field Hall effect gives the correct 2DEG parameters; at high temperatures where there is parallel conduction there is a slight discrepancy. The mobility spectrum analysis yields unphysically high sheet densities for the 2DEG at high temperatures.

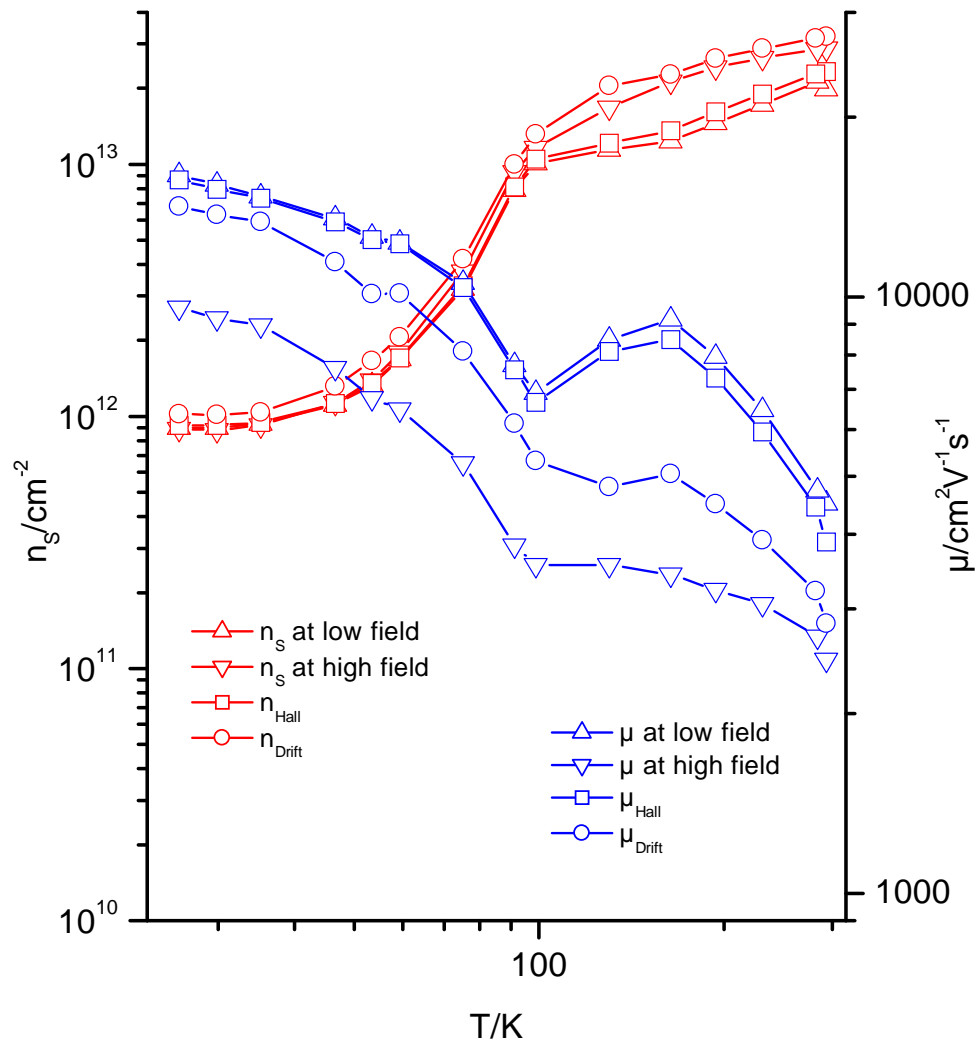


Figure 6.9 A summary of results extracted from magnetoresistance measurements. Mobilities and sheet densities measured directly using assumption of the single-carrier Hall effect at low magnetic field (where Equations 4.15, 4.17 and 4.18 should apply) and at high magnetic field (where 4.16 should apply, not applicable in the quantum limit) are shown, alongside results from the derived analyses of the spectrum, Equations 6.17, 6.18, 6.20 and 6.21. The calculated drift mobility should not be larger than the measured high field value: this is another sign that something may be wrong.

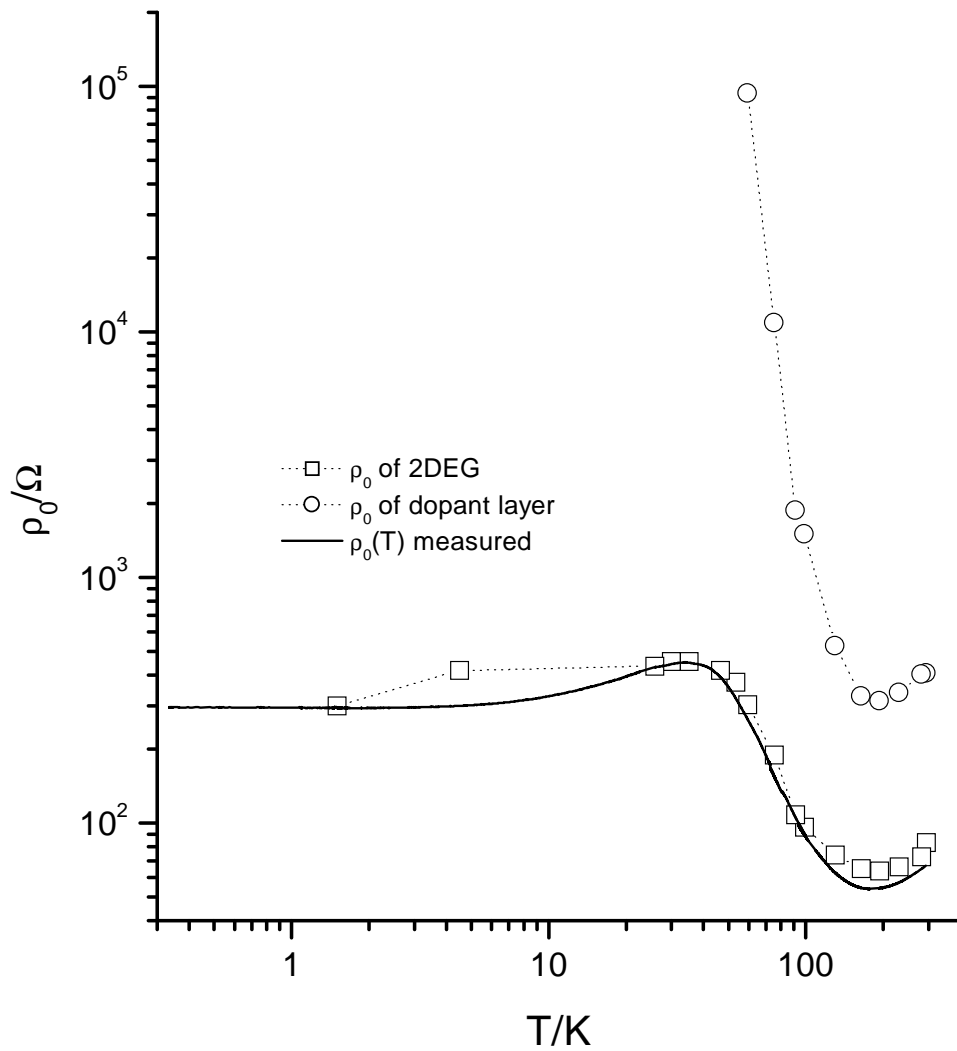


Figure 6.10 Dependence on temperature of the resistivity of the n-type device; directly measured data (at 150nA) is the solid line, symbols are results from mobility spectrum analysis. The Fermi temperature of the electron gas (calculated from its zero-temperature carrier concentration) is 70K, and it can be seen the the resistance is changing dramatically in this region. As the temperature decreases to a few Kelvin, the resistivity saturates. Freeze-out of the dopant layer can clearly be seen.

The Dopant Layer

The carrier concentration n_0 in the dopant layer as a function of temperature is:¹⁹

$$\frac{n_0(N_A + n_0)}{(N_D - N_A - n_0)} = \beta N_C \exp\left(\frac{-E_D}{k_B T}\right) \quad n_0 \ll N_C \quad 6.9$$

where N_D and N_A are the concentrations of donors and acceptors, N_C is the effective density of states in the conduction band and β is the degeneracy. N_C is given by:²⁰

$$N_C = 2 \left[\frac{2\pi m^* k_B T}{h^2} \right]^{3/2} \quad 6.10$$

If the $T^{3/2}$ dependence of N_C (and the temperature variation of the width of the ionized region of the dopant layer) is assumed to be much less important than the exponential temperature dependence in Equation 6.9, $n_0 \ll N_D$ and $N_D \gg N_A$ (as is likely since the concentrations used in modulation doping are very high compared to traditional device doping levels)²⁰ then Equation 6.9 reduces to:

$$n_0 \simeq A T^{3/4} \exp\left(-\frac{E_D}{2k_B T}\right) \quad 6.11$$

The temperature dependence of the sheet carrier density of the dopant layer (the red circles in Figure 6.8) in the region of 60-100K* suggests an activation energy of the arsenic donors of the order of the accepted value in pure silicon of 54meV,²¹ but since only a few data points are available a rigorous analysis is not possible. Since the dopant slab is only significantly ionized in the region nearest the active channel at these temperatures,²² this analysis cannot necessarily be used to infer the donor

* Data between 100K and 300K does not fit Equation 6.11 and cannot be used, for reasons which will be explored in the remainder of this chapter.

concentration.

The 2-Dimensional Electron Gas

Some variation of sheet density with temperature of the 2DEG is to be expected:¹¹ when $T \ll T_F$ the Fermi level is pinned in the dopant slab and the occupied quantum-well subband, similar to the case for p-type conduction shown in Figure 3.1. The charge density in the channel must be consistent with the gradient of the energy bands between the channel and the dopant slab (as discussed in section 6.3). At higher temperatures, the spreading of the Fermi occupation function means that the conduction band does not need to cross below the Fermi level to be significantly populated. However, such a large increase in 2DEG density as temperature increases may be a cause for some concern, and will be discussed in sections 6.5 and 6.8.2.

In strained silicon, the conduction band minimum is doubly degenerate. These two conduction valleys have identical mobilities and occupation densities, so in each case the 2DEG peak in the mobility spectra represents both sets of electrons. However, the density according to Shubnikov-de Haas oscillations will be half this, as will be seen.

"Mirror" Peaks

A very strong peak can be seen in the 4.5K spectrum, at a mobility of around $-14,000\text{cm}^2\text{V}^{-1}\text{s}^{-1}$. The effective sheet density of this peak is $(-)3.4 \times 10^{11}\text{cm}^{-2}$. This compares to the 2DEG peak, which has a mobility of $22,000\text{cm}^2\text{V}^{-1}\text{s}^{-1}$ at $6.8 \times 10^{11}\text{cm}^{-2}$. It can be seen immediately that this density for the 2DEG is too low (there is no reason for it to deviate from its value at other low temperatures of $9.0 \times 10^{11}\text{cm}^{-2}$) and that the missing conductivity is provided by the "mirror peak" which would, if it were genuine, represent p-type conduction. Spectra at 130K and 99K show very small peaks at low, negative mobilities; at other temperatures, similar peaks are present but with areas (that is, effective sheet densities) between two and four orders of magnitude lower than the genuine peaks. In fact, such very small mirror peaks result even from synthetic data

generated to test the software.

Mirror peaks (normally at exactly the opposite mobility value, unlike the peak seen in the 4.5K spectrum) are a general feature of mobility spectrum analysis, and have been described either as a computational artefact, a sign of band anisotropy or a result of inaccuracies in the measurement or processing of the ρ_{xx} signal.^{10,11,23} Only the first suggestion is consistent with mirror peaks even being present in spectra generated from synthetic data, but Reference 23 notes that they are a feature of analysis performed with different computational methods. Consider a mobility spectrum similar to the 4.5K result, with a well-defined and sharp real peak at μ_1 (with a total integrated conductivity of σ_1 and an effective carrier concentration of n_1) and a mirror peak at $\mu_2 = -\mu_1$. The magnetoconductivity is then given by

$$\sigma_{xx} = \int_{-\infty}^{+\infty} \frac{s(\mu) d\mu}{1 + \mu^2 B^2} = \frac{\sigma_1}{1 + \mu_1^2 B^2} + \frac{\sigma_2}{1 + \mu_2^2 B^2} = \frac{\sigma_1 + \sigma_2}{1 + \mu_1^2 B^2} \quad 6.12$$

$$\sigma_{xy} = \int_{-\infty}^{+\infty} \frac{\mu B s(\mu) d\mu}{1 + \mu^2 B^2} = \frac{\mu_1 B \sigma_1}{1 + \mu_1^2 B^2} + \frac{\mu_2 B \sigma_2}{1 + \mu_2^2 B^2} = \frac{(\sigma_1 - \sigma_2) \mu_1 B}{1 + \mu_1^2 B^2} \quad 6.13$$

If $n_2 \ll n_1$ then the conductivity, and therefore the resistivity, reverts to the single-carrier model. However, if $n_2 \sim n_1$ then the transverse component is reduced greatly. Since the longitudinal component is always normalized to match the data at zero field, the result of the mirror peak is to change the scale of σ_{xy} in relation to σ_{xx} without changing its form. This suggests that the mirror peak is a consequence of mis-match between the numerical values of the longitudinal and transverse elements of the conductivity tensor. In the case of real data, this may arise due to mis-calibration between the equipment that measures the longitudinal and transverse resistivities, numerical errors when inverting this to generate the conductivity, or rounding errors (data was exported as tab-separated text, with numbers in standard form to 6 significant figures). This latter applies even if the data is synthetically generated.

In conclusion, the presence of mirror peaks is a sign of suspect data that must be treated with care: calibration of experimental equipment and the methods in which the data is processed should be checked.

6.4.3 Obtaining Semiconductor Properties from a Mobility Spectrum

Sheet Density and Mobility

Traditionally, the extraction of semiconductor properties from the magnetoresistance is treated in terms of simple analytical functions such as are described in section 4.1.2. The Hall sheet density, for example, is defined as:

$$n_{Hall} = \frac{1}{q R_H (B \rightarrow 0)} \quad 6.14$$

where $R_H (B \rightarrow 0)$ is the Hall coefficient (Equation 4.14) at low magnetic field. It is acknowledged that the Hall coefficient at low fields is at the mercy of energy-dependent scattering within a carrier gas, or the presence of multiple carrier gases with differing mobilities.²⁴ In the limit of high magnetic field, however, the Hall coefficient should reflect only the total number of carriers within the system (Equations 4.16 and 4.21):

$$\sum |n| = n_{Drift} = \frac{1}{q R_H (B \rightarrow \infty)} \quad 6.15$$

The zero-field conductivity is $\sigma_0 = n_{Hall} q \mu_{Hall} = n_{Drift} q \mu_{Drift}$ and so the Hall and drift mobilities can be found.

A mobility spectrum $s(\mu)$ generally comprises one or more peaks. The centre of a peak i can be simply interpreted as the mobility μ_i of the carrier gas represented by the peak, and the concentration of carriers within the gas n_i can be found by integrating over the peak:

$$n_i q \mu_i = \sigma_i = \int s(\mu) d\mu \quad 6.16$$

with the normalization of the spectrum is such that $\sigma_0 = \sum_i \sigma_i = \int_{-\infty}^{\infty} s(\mu) d\mu$. The total number of carriers found by this method is the drift concentration:

$$n_{Drift} = \sum_i |n_i| \quad 6.17$$

And so the drift mobility is then:

$$\mu_{Drift} = \frac{\sigma_0}{n_{Drift} q} = \frac{\int s(\mu) d\mu}{q \sum |n_i|} \quad 6.18$$

However, since the Hall coefficient in the limit of zero magnetic field (from Equations 4.11 and 4.14, assuming $\sigma_{XY}^2 \ll \sigma_{XX}^2$ and $\mu B \ll 1$) is:

$$R_H(B \rightarrow 0) \simeq -\frac{1}{B} \frac{\sigma_{XY}}{\sigma_0^2} \simeq -\frac{1}{\sigma_0^2} \int \mu s(\mu) d\mu \quad 6.19$$

then the Hall concentration as defined in Equation 6.14 is found to be

$$n_{Hall} = \frac{\sigma_0^2}{q \int \mu s(\mu) d\mu} = \frac{\left(\int s(\mu) d\mu \right)^2}{q \int \mu s(\mu) d\mu} \quad 6.20$$

The Hall mobility is then

$$\mu_{Hall} = \sigma_0 R_H(B \rightarrow 0) = \frac{1}{\sigma_0} \int \mu s(\mu) d\mu = \frac{\int \mu s(\mu) d\mu}{\int s(\mu) d\mu} \quad 6.21$$

Hall Scattering Factor

The Hall scattering factor r is defined such that

$$R_H(B \rightarrow 0) = \frac{1}{n_{Hall} q} = \frac{r}{q \sum |n_i|} \quad 6.22$$

which leads to:

$$r = \frac{n_{Drift}}{n_{Hall}} = \frac{q \sum |n_i| \int \mu s(\mu) d\mu}{\left(\int s(\mu) d\mu \right)^2} \quad 6.23$$

In fact, a scattering factor can now be defined for each peak in the spectrum by limiting the integration to only the peak in question, rather than the whole spectrum:

$$r_i = q n_i \left(\int_{peak} \mu s(\mu) d\mu \right) \left(\int_{peak} s(\mu) d\mu \right)^{-2} \quad 6.24$$

Using the definition of n_i (Equation 6.16) this becomes:

$$r_i = \frac{1}{n_i q \mu_i^2} \int \mu s(\mu) d\mu \quad 6.25$$

Alternatively, since at high fields $\sigma_{XY}^2 \gg \sigma_{XX}^2$ and $\mu B \gg 1$:

$$R_H(B \rightarrow \infty) \simeq \frac{1}{B \sigma_{XY}} = \frac{1}{B} \left[\int \frac{\mu B s(\mu) d\mu}{1 + \mu^2 B^2} \right]^{-1} \simeq \left[\int \frac{s(\mu)}{\mu} d\mu \right]^{-1} \quad 6.26$$

from Equation 6.15 the drift concentration may be described as

$$n_{Drift} = \frac{1}{q} \int \frac{s(\mu)}{\mu} d\mu \quad 6.27$$

provided that $s(\mu=0)=0$, as it physically should be. The drift mobility is now

$$\mu_{Drift} = q \left(\int s(\mu) d\mu \right) \left(\int \frac{s(\mu)}{\mu} d\mu \right)^{-1} \quad 6.28$$

and the Hall scattering factor is:

$$r = \int \frac{s(\mu)}{\mu} d\mu \frac{\int \mu s(\mu) d\mu}{\left(\int s(\mu) d\mu \right)^2} \quad 6.29$$

(The integrals in Equations 6.27, 6.28 and 6.29 may be performed over individual peaks rather than the whole spectrum, as before.)

A Hall scattering factor greater than unity in a carrier gas is the result of energy-dependent scattering mechanisms, and according to Equation 6.25 a peak at μ_i will have r_i greater than unity if $\int \mu s(\mu) d\mu > \mu_i \int s(\mu) d\mu$. This will be the case for a symmetric, broad peak in the mobility spectrum. In order for a peak to have a Hall scattering factor less than unity, it is necessary for it to be asymmetric with most of its weight towards the origin. However, anisotropy in the energy band which leads to $r < 1$ is expected to produce "harmonics" in the mobility spectrum and Equation 6.25, which only considers a single peak, is not applicable.⁶

All of the significant peaks in the spectra shown Figures 6.5, 6.6 and 6.7 have a scattering factor of unity; small peaks which are thought to be artefacts tend to have unphysical values of r which are far from unity and sometimes even negative (and divergent between values calculated from Equations 6.25 and 6.29). Experience suggests that the shape of the peak in a mobility spectrum may owe as much to the quality of the data as to the scattering processes and band shape of the material, so

while the mobility of the 2DEG can be found despite parallel conduction in the dopant slab, little can be said about the link between energy-dependent scattering and mobility-dependent conductivity and therefore about the scattering mechanisms in non-degenerate semiconductors.

6.5 Resistivity and Mobility as a Function of Temperature

Figure 6.10 shows how the resistivity of the n-type device varies as a function of temperature at zero magnetic field, which should be compared with the variation of mobility and sheet density shown in Figure 6.8. The resistivity at room temperature is just over $60\Omega/\square$; at first the resistivity decreases slightly as temperature decreases from 300K, reaching a minimum around 200K, and then increases by almost an order of magnitude in the region of T_F to a peak at 30K. Resistivity then decreases to saturation at just under $300\Omega/\square$ as the temperature reaches 350mK. This data was obtained using a drive current of 150nA: the behaviour of the resistivity as a function of current at low temperatures is the subject of Figures 6.13 and 6.14 which are discussed in the next section.

Information from the mobility spectrum analysis (Figure 6.8) of the previous section suggests that the dominant contribution to the conductivity in this device is the 2DEG, even at high temperatures where the dopant slab has not frozen out.

There is a minimum in the resistivity at 160K which, since the sheet density is only increasing slowly in this range, corresponds to a maximum in the mobility. The decrease in mobility with temperature from here to 300K can be ascribed to acoustic phonon scattering: $\mu \propto T^{-\gamma}$ with $\gamma \sim 1$.²⁵ The room temperature value of the mobility in the 2DEG is $4,500\text{cm}^2\text{V}^{-1}\text{s}^{-1}$ (better than the room temperature electron mobility of bulk silicon of $1,400\text{cm}^2\text{V}^{-1}\text{s}^{-1}$)²¹ but the sheet density is unphysically high at $1.7 \times 10^{13}\text{cm}^{-2}$. The Hall scattering factor of the 2DEG (from Equations 6.25 and 6.29) is 1.0, so nothing can be inferred regarding scattering mechanisms.²⁶ Whilst some variation of sheet density with temperature is to be expected,¹¹ such a large variation

may be a sign of a problem with the magnetoresistance data, mobility spectrum theory, or the computer code performing the calculation. These possibilities will be discussed in section 6.8.2.

The change in resistivity between 160K and 40K is associated with the change in sheet density as the 2DEG becomes degenerate (and conduction in the dopant layer freezes out). However, inspection of the mobility spectrum results in Figure 6.8 shows how the mobility is at a minimum at 100K; the change in resistivity seen in Figure 6.10 appears to be, for temperatures between 100K and 160K, the result of changing mobility with a roughly constant sheet density. As the temperature falls below 100K, the mobility increases but the sheet density decreases such that the resistance variation is maintained: there is no significant feature visible in Figure 6.10 to mark the minimum in mobility. This minimum in mobility may be a real physical effect due to the temperature dependence of screening in the 2DEG,²⁷ but is more likely to be a sign that some part of the experimental procedure is awry. The mobility should probably continue monotonically decreasing as $\mu \propto T^{-1}$; the mobility and the density of the 2DEG are overestimated whenever the density in the dopant layer is significant.

The low temperature behaviour of the resistance is the subject of Figure 6.11. The mobility enhancement as the temperature decreases below 20K is most likely to be a quantum transport effect: the carrier gas is fully degenerate and the phonon scattering rate is very low.

There is little variation in the ~ 1 K region and no suggestion that the resistivity would tend to either zero or infinity at absolute zero. This can be compared with Figure 5.31 and the analysis in Section 5.5.3: $\rho(T)$ in a 2DHG with a sheet density of $1.07 \times 10^{12} \text{cm}^{-2}$ also decreases as temperature decreases below 20K, reaching a minimum and then increasing slowly and saturating.

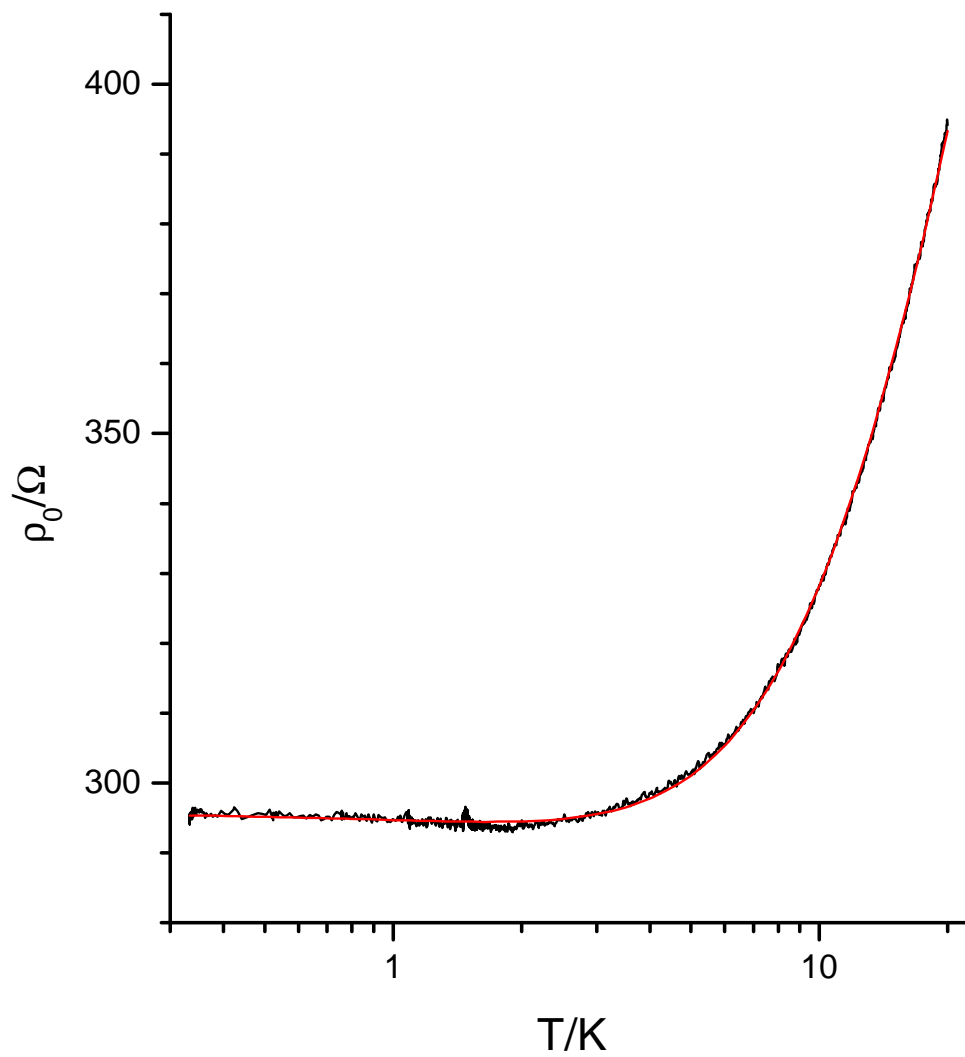


Figure 6.11 Calculated and measured resistivity as a function of temperature, to be compared with similar results in the previous chapter. Fitting parameters are given in the text.

Equation 5.15 was introduced to fit the $\rho(T)$ data shown in Figure 5.31: the results of fitting Equation 5.15 to the data in Figure 6.11 with n fixed at unity are $\rho_0=116\pm 1\Omega/\square$, $\rho_c=179\pm 1\Omega/\square$, $\rho_l=164\pm 2\Omega/\square$, $T_0=4.91\pm 0.04\text{K}$ and $\tau=1.65\pm 0.04\text{ps}$. This scattering rate corresponds to a mobility of $15,000\text{cm}^2\text{V}^{-1}\text{s}^{-1}$ which is close to the value of the mobility of the 2DEG at the peak in resistivity at 30K. Whether these fitting parameters relate to those shown in Figure 5.32 for a 2DHG is a subject for debate and investigation: the values of T_0 and τ from this 2DEG (at a density of $0.90\times 10^{12}\text{cm}^{-2}$) would not look out of place in the lower panel of Figure 5.32, but the resistivity parameters are clearly at least an order of magnitude smaller. Further discussion is presented in the conclusions of this chapter, section 6.8.2.

The low temperature maximum value of the mobility is $23,000\text{cm}^2\text{V}^{-1}\text{s}^{-1}$ at a sheet density of $9.0\times 10^{11}\text{cm}^{-2}$. This is typical for n-type strained silicon, not superlattice.^{25,28} Possible low-temperature mobility limiting mechanisms are discussed throughout the remainder of this chapter.

6.6 Quantum Hall Effect

6.6.1 Shubnikov-de Haas

Figure 6.12 shows a set of Shubnikov-de Haas oscillations at various temperatures, using a current of 150nA. For comparison, two additional results are shown at 350mK with different currents. Since the amplitude of Shubnikov-de Haas oscillations is the same at 150nA (black solid line) as at 30nA (black dotted line), there is no heating effect at 150nA. A current of 5 μ A (blue dotted line) heats the electron gas to over 2K. Using Equation 4.27 to extract the sheet density from the period of the oscillations in inverse magnetic field gives a result of $4.7\times 10^{11}\text{cm}^{-2}$ which is half the true value, found from the classical magnetoresistance, due to unresolved valley degeneracy.

A set of oscillations at 350mK at various currents is shown in Figure 6.13.

Figure 6.12 Shubnikov-de Haas oscillations as a function of temperature, at a current of 150nA. For comparison, two results at 350mK using different currents are shown. The sheet density found from the period of the oscillations in inverse magnetic field is $4.7 \times 10^{11} \text{cm}^{-2}$, which must be multiplied by two because of valley degeneracy. Spin degeneracy also applies at these field values, which is why the minima are at filling factors that are multiples of four. (See Section 4.1.3 and Figure 4.2)

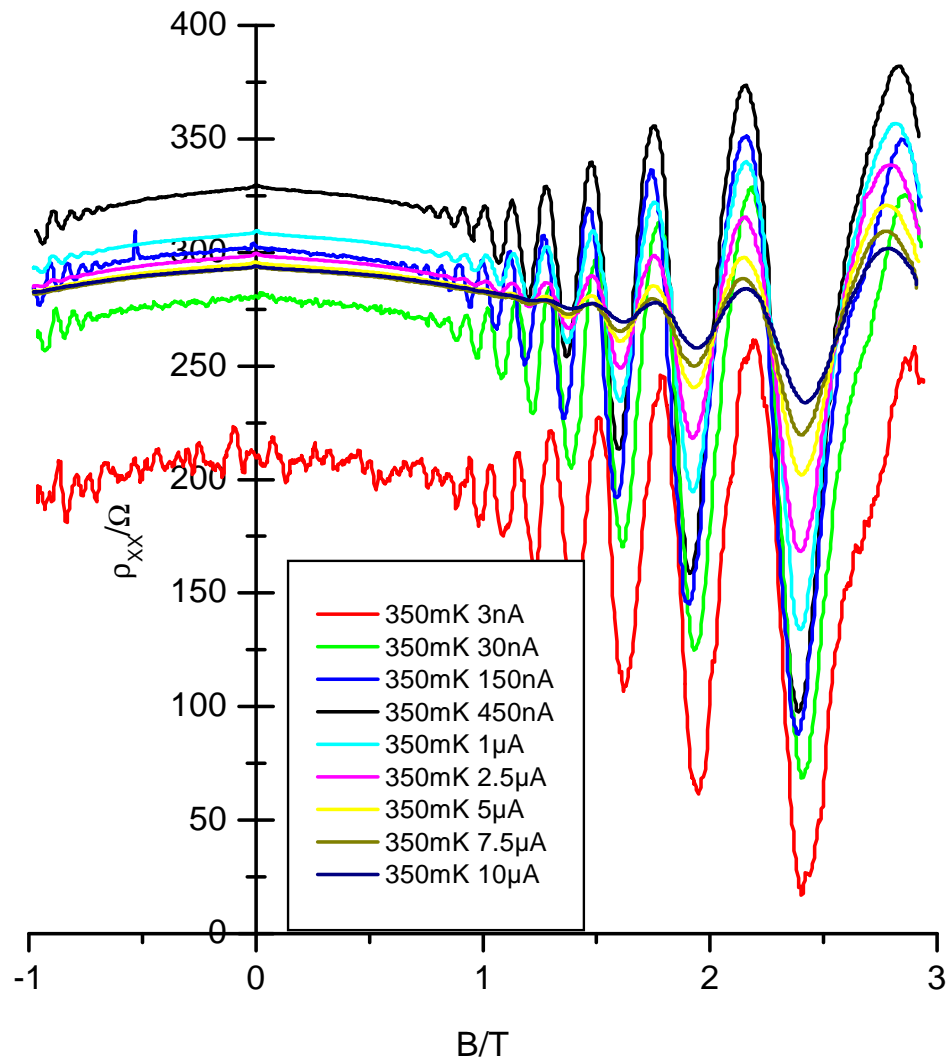


Figure 6.13 Shubnikov-de Haas oscillations as a function of current, at a temperature of 350mK. The zero-field value of the resistivity as a function of current is shown in Figure 6.14; the important notion here is that the amplitude of the oscillation is related to the temperature of the carrier gas (Equations 4.24 and 4.25) and there is no major decay in amplitude until the current reaches 1 μ A.

There is a large y-axis offset between the 3nA and the 150nA data, but no major reduction in the amplitudes of the oscillations until the current reaches 1 μ A. The oscillation amplitude as a function of current can be compared with the oscillation amplitude as a function of temperature to estimate the effective electron temperature as a function of current at a lattice temperature T_l of 350mK: at 1 μ A, $T_e \sim 1.2$ K and at 5 μ A, $T_e \sim 2.3$ K. The energy loss rate per electron as a function of electron temperature can be calculated:²⁹

$$\left\langle \frac{dE}{dt} \right\rangle = \frac{k_B (T_e - T_l)}{\tau_e} = \frac{\rho_{XX} I^2}{l^2 n_S} \quad 6.30$$

From this, the energy relaxation time τ_e and thence electron-phonon interaction strength can be found.^{25,29,30,31,32} Though this will not be pursued here, the energy relaxation time is relevant to the breakdown of the Quantum Hall state investigated in section 6.6.2. The data of Figure 6.13 reassures us that electron heating has not affected the Shubnikov-de Haas oscillation amplitudes in Figure 6.12.

The zero-field value of the resistivity as a function of current is plotted in Figure 6.14, which should be compared with Figure 6.11. Even though the resistivity seems lower at lower currents (which might suggest a heating effect) the fact that the variation in resistivity with temperature at these lower currents matches that shown in Figure 6.11 refutes this; the effect is more likely due to the difficulties with measuring such small signals. There is no variation of the low-field Hall coefficient with current.

The effective mass found from the temperature decay of the Shubnikov-de Haas oscillations in Figure 6.12 (using the method described in Section 4.1.3, particularly Equations 4.28 to 4.30) is $0.2m_e$ which is in agreement with the value of $0.199m_e$ from the calculations in Reference 3, presented in Section 6.3. The ratio of transport and quantum lifetimes, α , is 3.1.

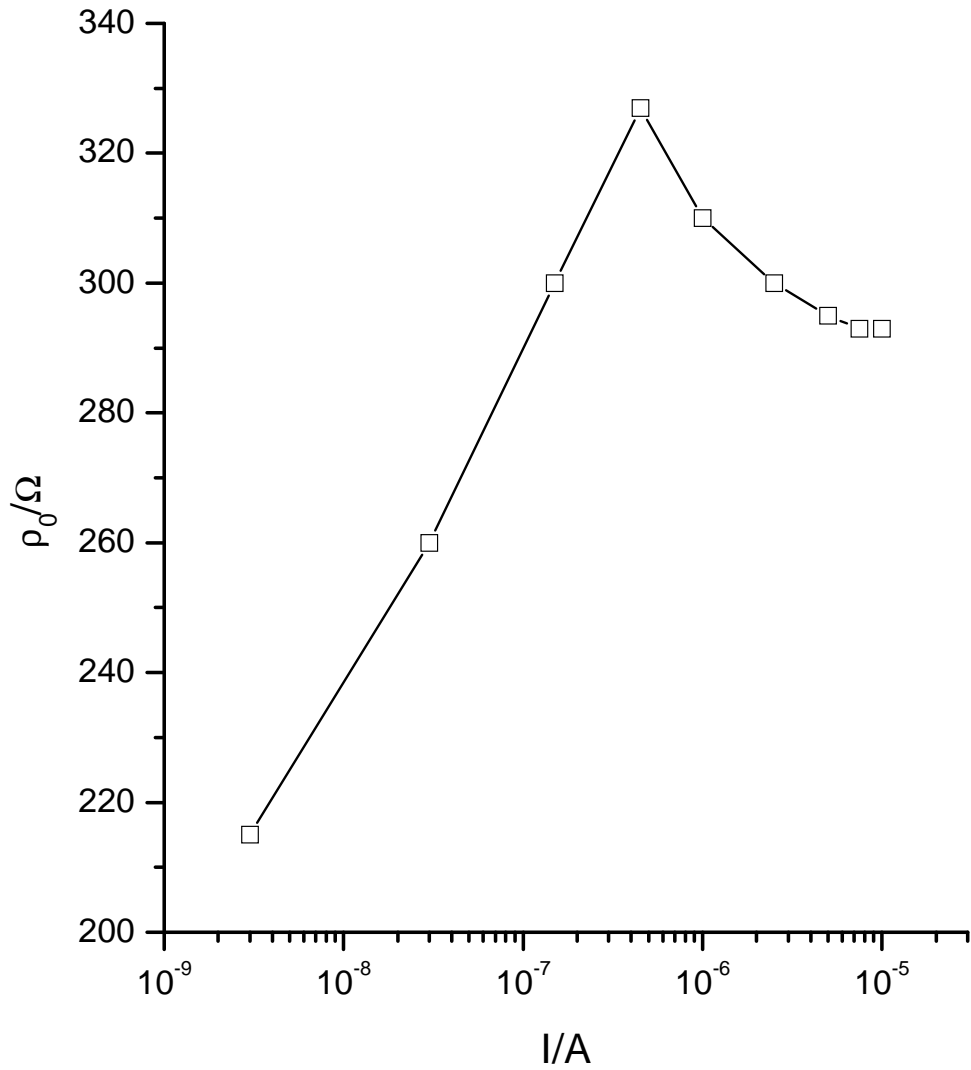


Figure 6.14 The zero-field value of the resistivity as a function of current. When compared to Figure 6.11 it is clear that the forms for the current and temperature dependent resistivity do not obviously map to each other.

In p-type silicon-germanium where interface impurities limit the mobility (commonly to around an order of magnitude less than the mobility of this 2DEG at a comparable sheet density, as seen in Chapter 5) the value of α tends to be around unity, indicating that scattering is short-range.³³ In heterostructures where the heterointerface is of very high quality and mobilities are over an order of magnitude higher than the mobility of this 2DEG, the value of α can be much larger: this indicates that most of the scattering in the system is small-angle, caused by ionized impurities which are remote from the 2DEG.³³ α values of up to 20 have been reported in very high mobility n-type silicon-germanium systems,^{34,35} comparable to that seen in high-quality heterostructures fabricated from other materials.³⁶

This value of α of 3.1, then, intuitively indicates a system where impurities both at and remote from the interface influence the mobility. Calculations in Reference 35 suggest that for a spacer of 15nm between the dopant slab and the active channel the value of α should be over 10 if interface impurities and roughness are ignored, which supports this conclusion. Calculations of the temperature dependence of the mobility, also from Reference 35, show that mobility increases slowly with decreasing temperature in the presence of interface impurities but that interface roughness causes the mobility to decrease with decreasing temperature. Figure 6.8 shows that therefore, interface impurities are limiting the mobility at low temperatures in this system.

Figure 6.15 (repeated from Figure 4.2) shows magnetoresistance data at 350mK up to 11T, which reaches a dissipationless state at the $\nu=4$ quantum Hall plateau. A full discussion is presented in Section 4.1.3. At around 3T the Shubnikov-de Haas oscillations with minima at $\nu=4n$ begin to break down. A minimum appears at $\nu=10$ as valley degeneracy is lifted, and a minimum appears at $\nu=5$ as spin degeneracy is lifted.

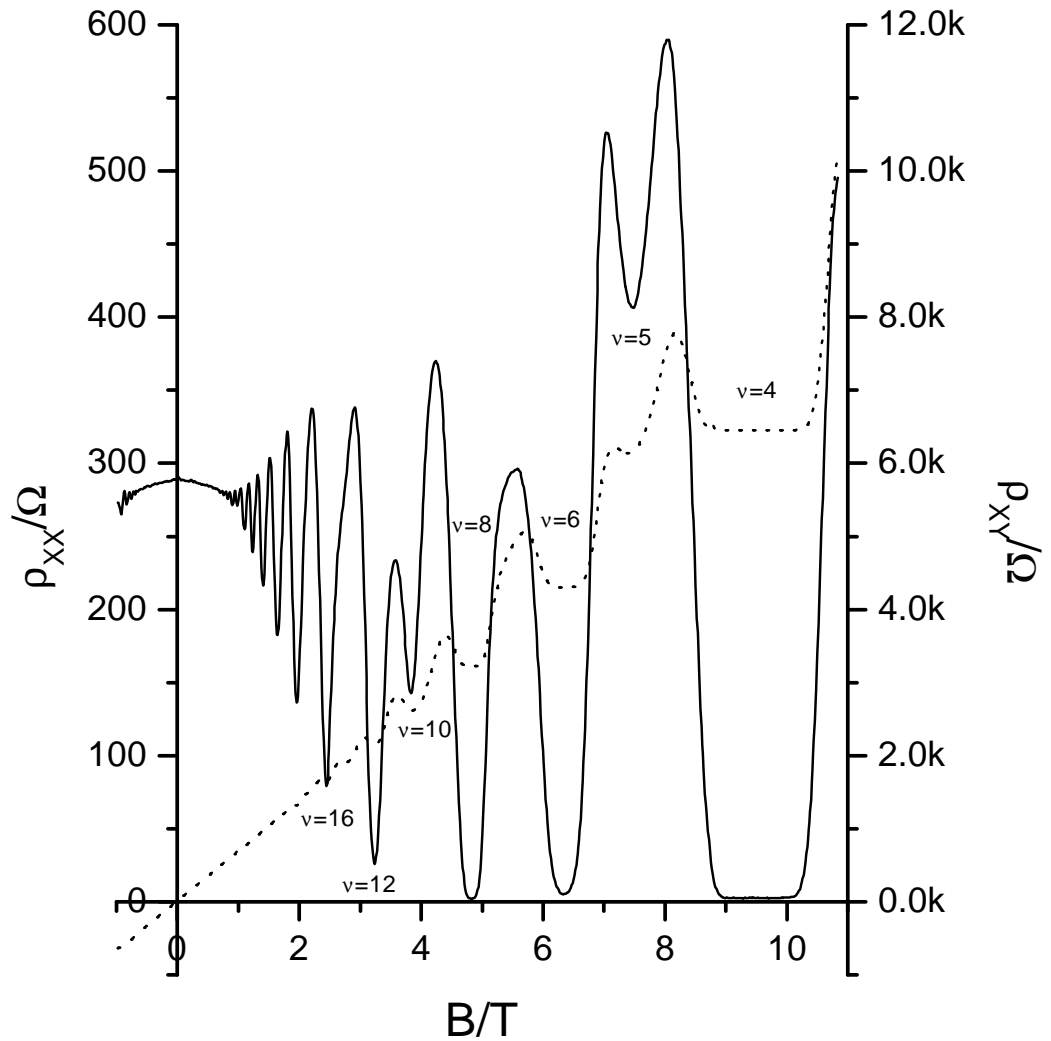


Figure 6.15 Shubnikov-de Haas and Quantum Hall Effects at a temperature of 350mK. The dotted line is the transverse resistivity and is associated with the y-axis on the right. Minima in resistivity are labelled with their corresponding filling factors. Conduction is dissipationless at $\nu=4$. The feature at $\nu=5$ corresponds to valley splitting, that at $\nu=10$ corresponds to spin splitting.

6.6.2 *IV at a Quantum Hall plateaux*

In Figure 6.16, data are presented which explore the current-voltage characteristics of the quantum Hall plateau state at 350mK, around the filling factor of 4. The dissipationless conduction ($\rho_{xx}=0$) makes this seem superficially similar to a superconducting state (in fact, there are similarities with the phase diagram of a Type II superconductor)^{37,38} but since the transverse element of the resistivity tensor has a finite value, $\rho_{xy}=h/(\nu e^2)$, then $\sigma_{xx}=0$ also. At the centre of this region, the dissipationless conduction breaks down at a critical current of around 3 μ A (the device is 1.75 μ m wide so the current density is 1.7Am⁻¹). For the highest filling factor shown, where the behaviour is almost Ohmic, the resistivity is around 500 Ω/\square .

The general characteristics and breakdown of the (integer) Quantum Hall Effect have been studied (mainly in n-type gallium arsenide and related systems) since it is exploited as quantum standard of resistance for use in metrology, and is also a system in which quantum phase transitions and interactions can be explored.^{39,40,41,42,43,44,45}

In Reference 43, the breakdown current density in n-type GaAs/AlGaAs at $\nu=2$ is around 0.5Am⁻¹ (a current of 210 μ A with through a Hall bar of width 0.4mm). Reference 42 finds that at $\nu=4$ the breakdown current density is 1.7Am⁻¹ (60 μ A through 35 μ m) decreasing to half this at $\nu=3.9$ and $\nu=4.1$. (Reference 45 finds that the breakdown current density in an InAs/GaSb crossed-gap electron-hole system is smaller by three orders of magnitude). The breakdown current decreases with filling factor and temperature in a manner similar to the phenomenological Gorter-Casimir two-fluid model for superconductivity.^{37,38}

There is no clear consensus on the mechanism for the breakdown of the Quantum Hall Effect. Indeed, it may be the case that there are two or more unrelated mechanisms.^{39,40,43} Breakdown can occur as a sequence of regular steps in longitudinal voltage, with heights of a few millivolts, and this has been linked to tunnelling between Landau level edge states.⁴³ No such steps were observed in this system.

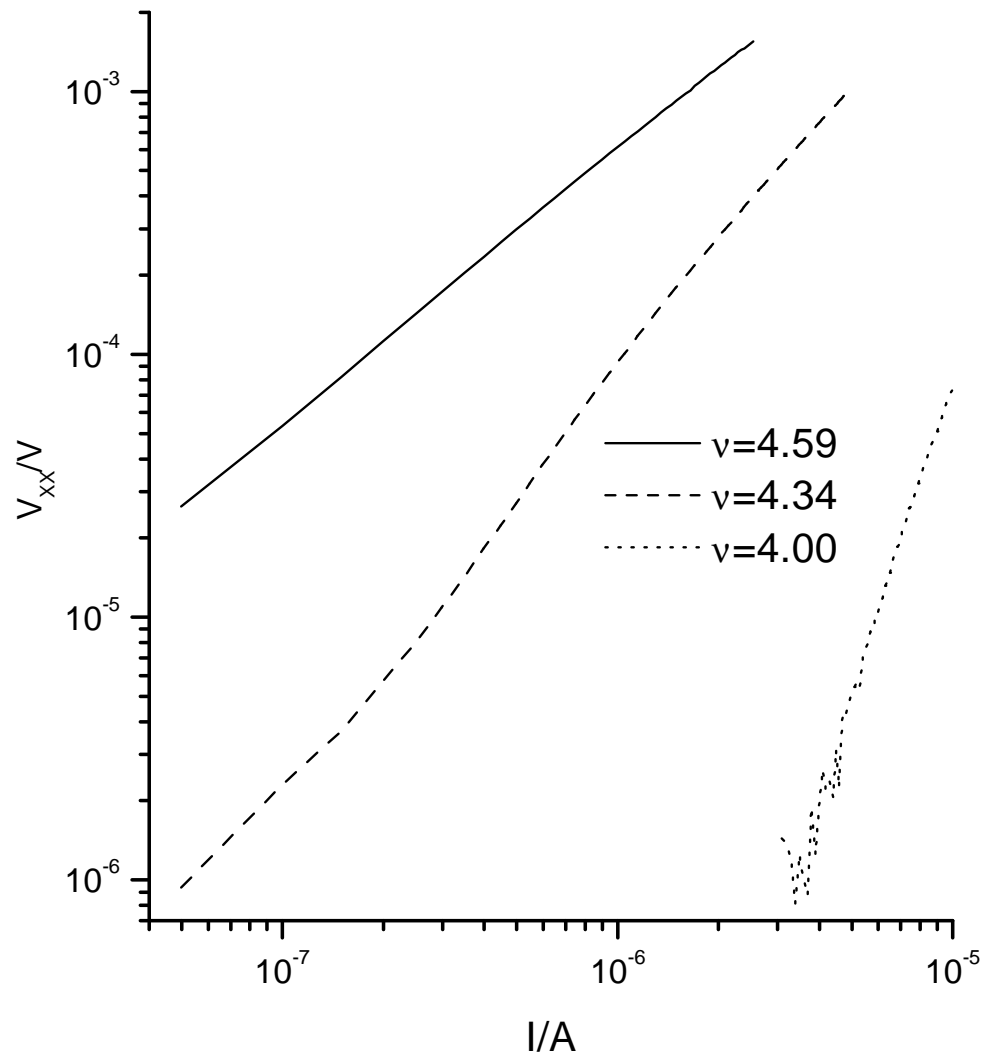


Figure 6.16 IV data taken close to the dissipationless state at the $\nu=4$ quantum Hall plateau. At $\nu=4$ itself, there is essentially no voltage drop (that is discernable above the noise floor) along the sample until a critical current of $3\mu\text{A}$ is applied. At higher filling factors (lower fields) there are decreasing deviations from perfect Ohmic behaviour.

A "bootstrap" self-heating mechanism is proposed in Reference 40, where the Quantum Hall Effect undergoes avalanche breakdown when the transverse electric field reaches a

critical value of $E_b = \sqrt{\frac{2\hbar}{m^* \tau_e}} B$. Using (from section 4.1.3) $\rho_{XY} = \frac{V_{XY}}{I} = \frac{E_y w}{I} = \frac{h}{\nu e^2}$

and $n_S = \nu B/h$ the breakdown current density is:

$$\frac{I_b}{w} = n_S e \sqrt{\frac{2\hbar}{m^* \tau_e}} \quad 6.31$$

The energy relaxation time τ_e (Equation 6.30, found by comparing the temperature and current dependence of the amplitude of Shubnikov-de Haas oscillations in Figures 6.12 and 6.13) is $\sim 10^{-8}$ s so the breakdown current density is estimated to be 0.5 Am^{-1} . To obtain the measured value of 1.7 Am^{-1} τ_e would need to be less than 10^{-9} s. Nevertheless, this agreement is good and may be improved by more rigorous determination of τ_e .

6.7 The Effects of Infra-Red Radiation

6.7.1 Shubnikov-de Haas

Figure 6.17 demonstrates the effect of illuminating the sample with a gallium-arsenide infra-red light emitting diode at 350mK. It can be seen that the illumination increases the resistance at zero field, and changes the Hall coefficient and the period of the oscillations. The amplitude of the oscillations does not decrease, showing that there are no heating effects. The ratio of quantum and transport lifetimes, α , is 3.6 during the illumination (slightly larger than before) and the changes in sheet carrier concentration are summarized in Table 6.1. While the sample is being illuminated, carriers appear to be driven out of the conducting channel. Following illumination some, but not all, return. The mobility appears to change in line with the density.

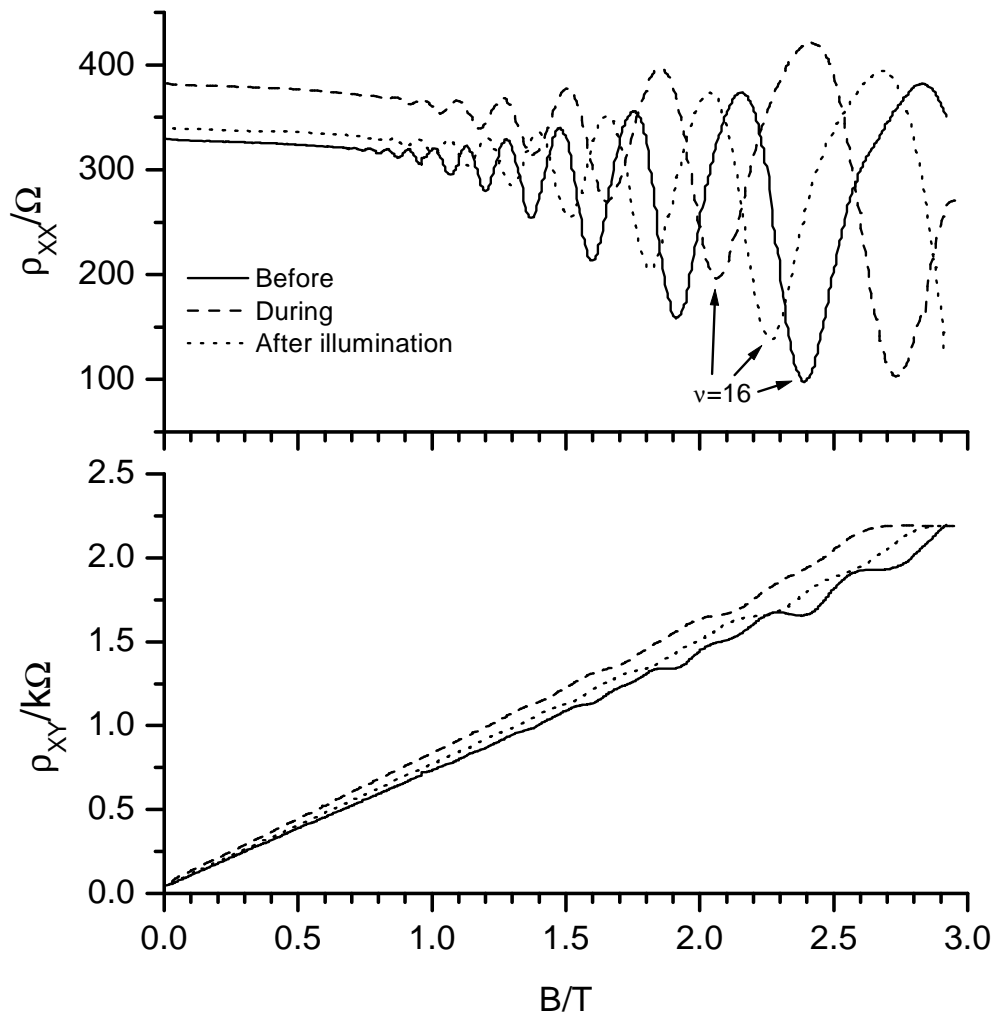


Figure 6.17 Magnetoresistance results at 350mK, showing the effects of illumination by infra-red radiation.

The low-field magnetoresistance (before oscillations begin: high-field magnetoresistance can not be used to explore the mobility spectrum in the presence of Landau levels) does not suggest that any parallel conduction channels are formed by the action of the light: even though the zero-field value of the resistivity is changed, the form of the magnetoresistance is identical. Parallel conduction would be apparent as a change in the gradient of $\rho_{xx}(B)$ with magnetic field, as can be seen in Figure 4.1.

<i>Sheet Density / 10^{11}cm^{-2}</i>	<i>Hall</i>	<i>Shubnikov-de Haas</i>
Before:	8.8	9.4
During:	8.0	7.6
After:	8.5	8.8

Table 6.1 A summary of the changes in carrier concentration in response to infra-red light, from Figure 6.17. The Hall results are calculated from the gradient of $\rho_{xy}(B)$ using Equation 4.7 and the Shubnikov-de Haas results are calculated from the period of the oscillations of $\rho_{xx}(B)$ in inverse magnetic field using Equation 4.27, including a factor of 2 for valley degeneracy.

6.7.2 Resistance as a Function of Temperature

Two results are presented in Figure 6.18: the continuous set shows how the resistivity varies with temperature for the device under illumination compared to the device in the dark, as it was cooled. The points joined by lines were taken at stable temperatures, with the device subjected to periods of illumination to observe how its resistivity changed with time. The transient at the beginning of the period of illumination was always very sharp, but the fall-off at the cessation of illumination showed a finite decay time, particularly at low temperatures. As Figure 6.19 shows, at 4.2K a decay time of the order of 100 seconds was identified, this falls rapidly to the order of 10 seconds at 10K and then becomes too short to discern behind the 3 second time constant of the measuring equipment. The energy involved is therefore roughly the value of $k_B T$ at 10K, $\sim 1 \text{meV}$.

At temperatures less than 10K, the irradiation simply increases the resistivity of the device by reducing both the sheet carrier concentration and the mobility.

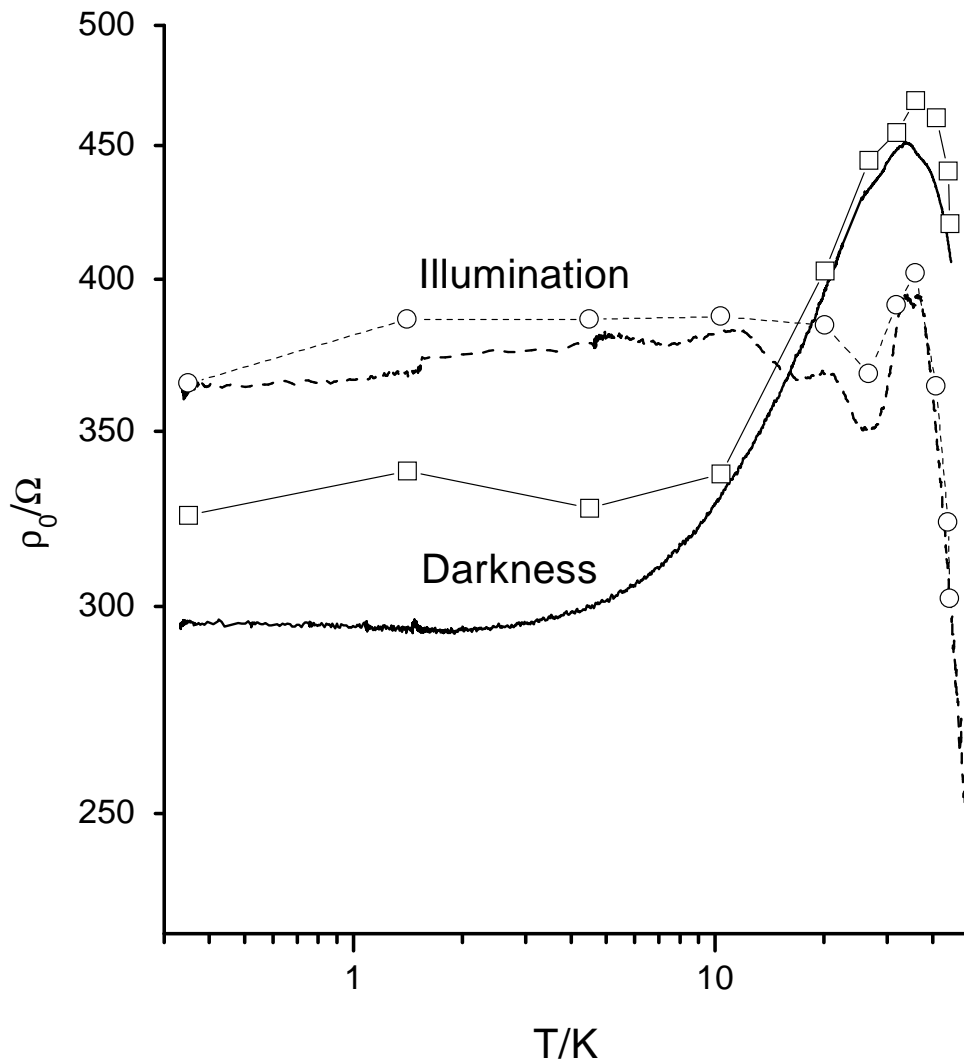


Figure 6.18 The resistivity as a function of temperature, demonstrating the effects of infra-red radiation. The continuous traces were taken by cooling the device under constant (illuminated or dark) conditions; the points joined by lines show results taken at stabilized temperature values with intermittent illumination.

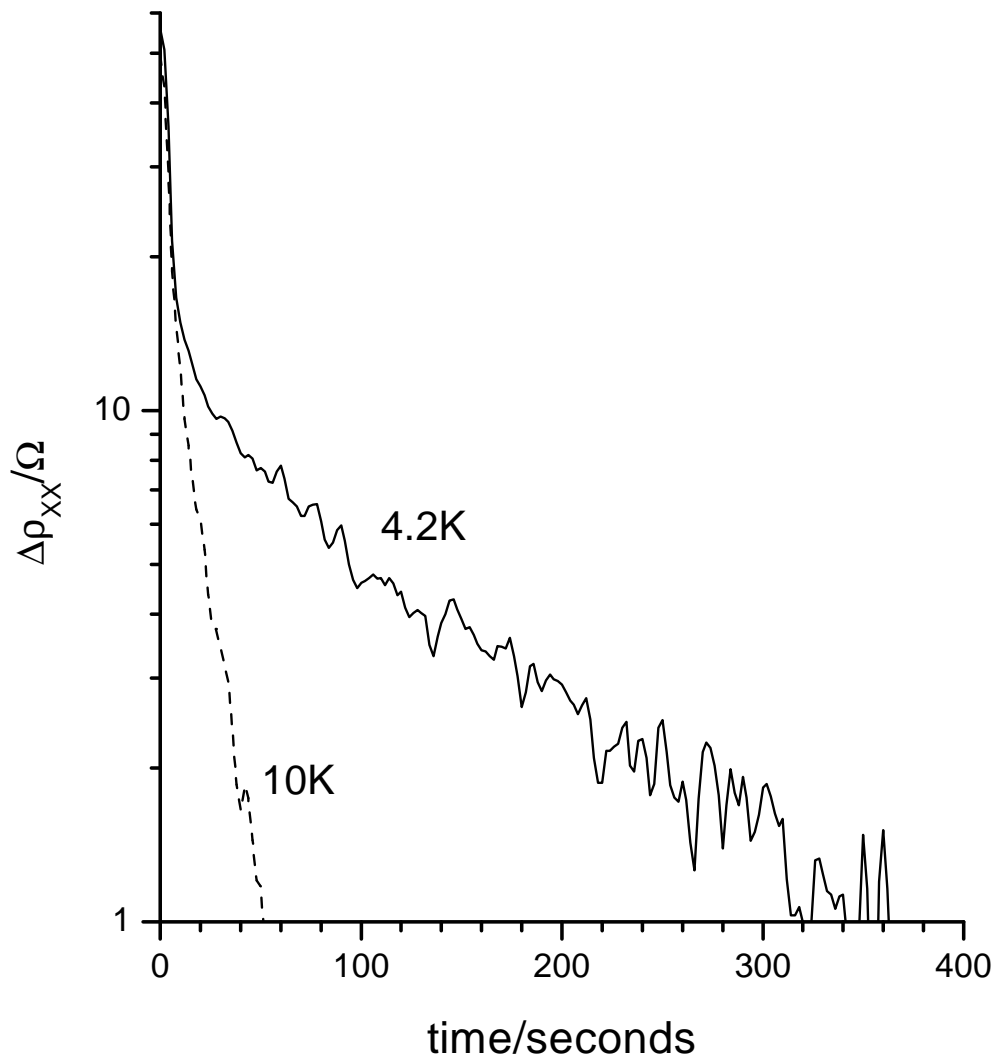


Figure 6.19 The resistivity as a function of time, demonstrating the effects of infra-red radiation. At time zero, illumination ceases, and the value of resistivity decays back to its dark value. At 4.2K, the decay is much more persistent than at 10K.

Since there is no evidence from the magnetoresistance for the formation of a parallel conduction channel of a mobility comparable to that of the 2DEG, and such a channel would tend to decrease the resistivity of the whole device, then the simplest interpretation is that the radiation causes 10% of the carriers to become unavailable for transport. The energy from the radiation clearly perturbs the equilibrium position (which then takes of the order of at least a few hundred seconds to become re-established) so it is possible that carriers are caused to move out of the quantum well and into the alloy spacer layer, where they are drawn towards ionized donor atoms. Upon cessation of the radiation, equilibrium is re-established.

The associated slight reduction in screening may be the cause of the increase in scattering rate. The slight increase in α suggests that the screening effects are more effective for the remote impurities than the local (interface) impurities, since large α values suggest remote impurity scattering, whereas $\alpha \sim 1$ is characteristic of scattering from impurities at the heterointerface where the 2DCG is defined.

Above 20K, the radiation tends to reduce the resistivity. The sharp fall-off which begins at around 40K parallels that which occurs in the device, in the dark, around the Fermi temperature; this is consistent with the reduction in the 2DEG carrier concentration and the consequent reduction in T_F .

The region between 15K and 40K is more interesting, showing what appear to be local minima and maxima in resistivity, and may be worthy of more investigation, particularly since the formation of Landau levels will be suppressed at this temperature so that mobility spectrum analysis may discover a low-mobility parallel conduction channel. At room temperature, there is no noticeable response to illumination.

6.8 Conclusion

6.8.1 Mobility and Resistivity

The mobility of the electrons in the 2DEG of this n-channel device is understandably superior to that of the holes in the p-channel devices discussed in the previous chapter. At room temperature, their mobility is also superior to the electrons in an n-channel MOSFET or indeed in bulk silicon, according to both low-field Hall effect and mobility spectrum analysis.

Since the effective mass difference alone cannot account for this (that of the electrons here is $0.2m_e$ whereas the holes in the previous chapter were found to have an effective mass of around $0.3m_e$) the scattering time must be mainly responsible.

The low resistivity of the device at low temperatures leads (via Equation 5.1) to a very high k_{Fl} value of almost 100, which (via Equation 5.2) suggests a dephasing time at 1K of over 100ps. The low-field magnetoresistance at very low temperatures shows no evidence for weak-localization (as seen in Figure 5.10) which suggests that $\tau_\psi \sim \tau$.

An elastic scattering time as long as this could only be the result of an extremely low impurity density in the active channel, and a very smooth interface, compared to characteristic p-channel devices. This is backed-up by the ratio of quantum and transport lifetimes found from the field dependence of the amplitudes of the Shubnikov-de Haas oscillations being larger than one. Also, the fact that when infra-red radiation is used to reduce the sheet carrier density the mobility also decreases, suggests that the mobility is limited by screened interface impurities rather than by interface roughness.

The high quality of the interface may be due to the normal structure of the device, with the dopant slab grown after the active channel and therefore with less time to diffuse into it compared to inverted structures. However, a gated HMOS device would either be inverted or not be modulation doped at all.

The form of the resistivity at low temperature, shown in Figure 6.11, is similar to the result in Figure 5.31 for the Siemens device at a sheet density of $1.1 \times 10^{12} \text{cm}^{-2}$ (which is the closest sheet density to the 2DEG). There is a weak minimum in resistivity at 2K but as temperature continues to decrease the resistivity appears to be saturating. Equation 5.15 has been fit to the data, but with $n=1$. Much more work would be necessary to establish any physical justification for the applicability of Equation 5.15 to the data in Figure 6.11.

6.8.2 Mobility Spectrum Analysis

Methodology

Mobility spectrum analysis is a general technique that should be applicable to any system where the mobility of the charge carriers is not a function of magnetic field. The lower limit of mobility than can be reliably found is roughly the reciprocal of the maximum magnetic field that the data extends to; the upper limit is the reciprocal of the spacing between the data points in inverse magnetic field.

In semiconducting samples and cryomagnetic systems, the upper limit is practically set so that the resulting mobility spectrum is detailed enough in the region where carriers are expected to be found but does not waste points elsewhere. However, the lower limit is often a serious issue. Hence, this analysis method is much easier to test on an n-channel device such as this, compared to a p-channel device which may have a mobility smaller by a factor of 5 or 10.

Many mobility spectrum analysis methods do not respond well to large numbers of data points (requiring human choices of which data points to keep and which to discard) or employ tricks, assumptions, interpolations or extrapolations in order to recondition the data or guide the solution. A new method is presented here (Bryan' s Algorithm Mobility Spectrum: *BAMS*) which uses singular value decomposition to remove noise and overspecification from the data set and the principles of Bayesian inference and Bryan' s algorithm maximum entropy to find a mobility spectrum. (It is

quite distinct from the maximum entropy mobility spectrum method in Reference 11).

Singular value decomposition carries out two essential tasks: firstly, by removing overspecification from the data (that is, by finding lines within the matrix which are linear combinations of each other) the basis space which must be searched for a solution is reduced dramatically. Secondly, by discarding elements of the matrix which are smaller than the noise floor, the inversion is protected against the tendency to fit very well to features of the data which are noise at the expense of the underlying, physical data.

The maximum entropy method also performs two functions. Firstly, since the use of a default model allows information about the expected solution to be added in, setting a positive and normalizable default model which has a constant value across the whole spectrum ensures (due to the logarithmic form of the entropic regularization) that the resulting mobility spectrum will be positive and normalizable. Secondly, the hyper-parameter α nominates the relative importance of a very good least-squares fit to the data versus a physically reasonable spectrum which contains as much information as it is reasonable to extract from the data without introducing spurious artefacts.

Bryan's algorithm chooses solutions which are the most probable regarding the value of the hyper-parameter, and the refinement of this method by Hague (use of a solution as the default model to find a better solution) ensures that the final value of the hyper-parameter is well within the bounds of the applicability of Bryan's algorithm.

One drawback with the maximum entropy technique is that it is very important to have an accurate estimation of the error in the experimental data. Tests with synthetic data, however, lead to the conclusion that overestimation of the error acts on the solution in an intuitive way, broadening peaks and washing out fine detail; underestimation of the error leads to solutions which can be rejected due to their obvious unphysicality. Whilst this is clearly not satisfactory (we would like to always achieve the best result possible and trust what we find) there has been no cause to worry that results which appear physical but are wrong are likely to be produced by

mistakenly assuming a certain error level. A more analytical treatment of the level of error is an important line for further work, but the human process of rejecting data which is errant because of equipment mis-calibrations or failures will always be necessary.

Methods of obtaining classically measured quantities from a mobility spectrum have been described, and although mobility spectra are rarely of such good resolution that the Hall scattering factor can be unambiguously found, these analyses at least provide a check for unphysicality. It has been argued that a common feature in mobility spectra, the "mirror peak," is an artefact due to discrepancy between the relative values of the longitudinal and transverse values of the conductivity tensor.

Results

The results produced by the mobility spectrum analysis, shown in Figures 6.5 to 6.10, are feasible at low temperature but seem to become anomalous as temperature increases. The low temperature 2DEG sheet density agrees with calculations (see section 6.3) but the room temperature sheet density (nearly 20 times greater than this) is not supported by simulation of the band profile using a numerical solution of the Poisson equation. In fact, the room temperature 2DEG density should be much closer to its low temperature density.¹¹ However, to maintain the same conductivity at such a density would require ridiculously high mobility.

The sheet density of the dopant layer was found to reach $1.5 \times 10^{13} \text{cm}^{-2}$ at room temperature. Since the doping slab is 30nm thick, this corresponds to an average carrier concentration of $5 \times 10^{18} \text{cm}^{-3}$ and this value is typical for the donor concentration in modulation doping. However, the mobility of the dopant layer was found to be $1000 \text{cm}^2 \text{V}^{-1} \text{s}^{-1}$ meaning that overall its resistance was $400 \Omega/\square$. For a 30nm thick layer, this corresponds to a resistivity of $10^{-3} \Omega \text{cm}$. To achieve such low resistivities the donor concentration must be almost 10^{20}cm^{-3} since the mobility of a doped semiconductor generally decreases with the doping dose.^{20,21,46} In other words, the mobility of the dopant layer returned by this mobility spectrum analysis is

probably too high.

However, to ascribe less of the device' s conduction at room temperature to the dopant layer (by reducing its mobility without increasing its sheet density) means that either the mobility or density of the 2DEG must be increased and these two parameters are already worryingly large. According to *BAMS* there are no other conducting channels within the range $|\mu| \leq 10 \text{m}^2 \text{V}^{-1} \text{s}^{-1}$.

Other established analyses yield similar results for mobility and sheet density of the 2DEG and dopant layer; *BAMS* analysis of other magnetoresistance data from p-channel systems yields more reasonable results, with the 2DHG density varying by less than 20% between 50K and 300K. This means that it is unlikely that there is a problem with the *BAMS* code. Also, even though mobility spectrum theory is possibly not as useful in a quantitative way as was originally hoped⁶ (since it says little about the energy dependence of the relaxation time) it has proved its worth in a qualitative or semi-quantitative way, finding feasible mobility and sheet density results in many cases.

The issue seems to be that the room temperature resistance of the device is only $70 \Omega/\square$, and the only way in which the resistance can be so low is for there to be a large number of mobile carriers. Since the low temperature results are feasible it is unlikely that the measurement system itself is at fault, and so there is no reason to suspect that the observed drop in resistance of almost an order of magnitude between 30K and 100K is real. Also, *BAMS* tends to reject unphysical data outright, without returning any solution.

There may be, then, bulk conduction throughout much of the substrate through current paths which undermine the simple conversion of V_{XX} and V_{XY} to elements of the resistivity tensor of the device.

As for finding the energy dependence of the scattering time, more directly related to the scattering mechanisms limiting transport than the mobility on its own, a method based on the sheet density and/or temperature dependence of the mobility

(obtained by *BAMS* if necessary) may probably be more promising than attempting to analyze the mobility spectrum peak shape.

6.8.3 *Other Results*

The IV characteristics of a dissipationless $\rho_{xx} = \sigma_{xx} = 0$ quantum Hall state have been briefly investigated. At exactly $\nu = 4$ the dissipationless state breaks down at a current of $3\mu\text{A}$; as ν is increased linear Ohmic behaviour is eventually recovered. The response of the device to infra-red radiation is also explored: at very low temperatures the free carrier density is reduced, the mobility drops, and α increases. This correspondence is seen as evidence that it is screened interface and remote impurities that limit the mobility, not interface roughness.

- 1 F. Schäffler, *High-mobility Si and Ge structures*, Semiconductor Science and Technology **12** 1515-1549 (1997)
- 2 M. A. Sadeghzadeh, C. P. Parry, P. J. Phillips, E. H. C. Parker and T. E. Whall, *Issues on the molecular-beam epitaxial growth of p-SiGe inverted-modulation-doped structures*, Applied Physics Letters **74** (4) 579-581 (1999)
- 3 M. M. Rieger and P. Vogl, *Electronic-band parameters in strained $Si_{1-x}Ge_x$ alloys on $Si_{1-y}Ge_y$ substrates*, Physical Review B **48** (19) 14276-14287 (1993)
- 4 Z. Dzuiba, T. Przeslawski, K. Dybko, M. Górka, J. Marczewski and K. Regiński, *Negative magnetoresistance and impurity band conduction in an $In_{0.53}Ga_{0.47}As/InP$ heterostructure*, Journal of Applied Physics **85** (9) 6619-6624 (1999)
- 5 S. A. Studenikin, A. V. Chaplik, I. A. Panaev, G. Salis, K. Ensslin, K. Maranowski and A. C. Gossard, *Classical magnetotransport in a parabolic quantum well with a strong intersubband scattering*, Semiconductor Science and Technology **14** 604-610 (1999)
- 6 W. A. Beck and J. R. Anderson, *Determination of electrical properties using a novel magnetic field-dependent Hall technique*, Journal of Applied Physics **62** (2) 541-554 (1987)
- 7 J. S. Kim, D. G. Seiler and W. F. Tseng, *Multicarrier characterization method for extracting mobilities and carrier densities of semiconductors from variable magnetic field measurements*, Journal of Applied Physics **73** (12) 8324-8335 (1993)
- 8 K. Regiński, J. Marczewski, Z. Dziuba and E. Grodzicka, *Mobility spectrum approach in the analysis of the eptaxial conduction of a GaAs layer grown by molecular beam epitaxy*, Journal of Applied Physics **82** (12) 6102-6106
- 9 J. R. Meyer, C. A. Hoffman, J. Antoszewski and L. Faraone, *Quantitative mobility spectrum analysis of multicarrier conduction in semiconductors*, Journal of Applied Physics **81** (2) 709-713 (1997)
- 10 I. Vurgaftman, J. R. Meyer, C. A. Hoffman, D. Redfern, J. Antoszewski, L. Faraone and J. R. Lindemuth, *Improved quantitative mobility spectrum analysis for Hall characterization*, Journal of Applied Physics **84** (9) 4966-4973 (1998)
- 11 S. Kiatgamolchai, *Maximum-Entropy Mobility Spectrum of Two-Dimensional Hole Gas in Strained- $Si_{1-x}Ge_x/Si$ Heterostructures*, Thesis, University of Warwick (2000)
- 12 D. S. Sivia, *Bayesian Inductive Inference, Maximum Entropy, and Neutron Scattering*, Los Alamos Science (19) 180-205 (1990)
- 13 M. Jarrell and J. E. Gubernatis, *Bayesian inference and the analytic continuation of imaginary-time quantum Monte Carlo data*, Physics Reports **269** 133-195 (1996)
- 14 J. P. Hague, *Band to Mott transition in the infinite-dimensional Holstein model*, Thesis, University of Warwick (2001)

-
- 15 E. T. Jaynes, *Information Theory and Statistical Mechanics*, Physical Review **106** (4) 620-630 (1957)
- 16 J. E. Gubernatis, M. Jarrell, R. N. Silver and D. S. Sivia, *Quantum Monte Carlo simulations and maximum entropy: Dynamics from imaginary-time data*, Physical Review B **44** (12) 6011-6029 (1991)
- 17 E. Gallicchio and B. J. Berne, *On the calculation of dynamical properties of solvated electrons by maximum entropy analytic continuation of path integral Monte Carlo data*, Journal of Chemical Physics **105** (16) 7064-7078
- 18 W. H. Press, S. A. Teukolsky, W. T. Vetterling, B. P. Flannery, *Numerical Recipes in C*, Cambridge University Press (1988, 1992)
- 19 J. S. Blakemore, *Solid State Physics*, Cambridge University Press (1974)
- 20 S. M. Sze, *Semiconductor Devices: Physics and Technology*, Wiley (1985)
- 21 M. Levinshtein, S. Rumyantsev and M. Shur, *Semiconductor Parameters Volume 1*, World Scientific (1996)
- 22 C. J. Emeleus, T. E. Whall, D. W. Smith, R. A. Kubiak, E. H. C. Parker and M. J. Kearney, *Scattering mechanisms affecting hole transport in remote-doped Si/SiGe heterostructures*, Journal of Applied Physics **73** (8) 3852-3856 (1993)
- 23 J. Achard, C. Varenne-Guillot, F. Barbarin, M. Dugay, *Comments on the appearance of "mirror" peaks in mobility spectrum analysis of semiconducting devices*, Applied Surface Science **158** 345-352 (2000)
- 24 J. S. Kim, *A matrix formalism for the Hall effect in multicarrier semiconductor systems*, Journal of Applied Physics **86** (6) 3187-3194 (1999)
- 25 S. Madhavi, V. Venkataraman, J. C. Sturm and Y. H. Xie, *Low- and high-field transport properties of modulation-doped Si/SiGe and Ge/SiGe heterostructures: Effect of phonon confinement in germanium quantum wells*, Physical Review B **61** (24) 16807-16818 (2000)
- 26 E. H. Putley, *The Hall Effect and Related Phenomena*, Butterworth & Co. (1960)
- 27 H. Sakaki, T. Noda, K. Hirakawa, M. Tanaka, and T. Matsusue, *Interface roughness scattering in GaAs/AlAs quantum wells*, Applied Physics Letters **51** (23) 1934-1936 (1987)
- 28 D. J. Paul, A. Ahmed, M. Pepper, A. C. Churchill, D. J. Robbins, D. J. Wallis and A. J. Pidduck, *Electrical properties and uniformity of two dimensional electron gases grown on cleaned SiGe virtual substrates*, Journal of Vacuum Science and Technology B **16** (3) 1644-1647 (1998)
- 29 G. Braithwaite, *Characterisation of the Hole-Acoustic Phonon Interaction in Modulation Doped Si/Si_{1-x}Ge_x (0.085 ≤ x ≤ 0.28) Heterostructures*, Thesis, University of Warwick (1999)
- 30 G. Stöger, G. Brunthaler, G. Bauer, K. Ismail, B. S. Meyerson, J. Lutz and F. Kuchar, *Shubnikov-de Haas oscillations and negative magnetoresistance under hot-electron conditions in Si/SiGe heterostructures*, Semiconductor Science and Technology **9** 765-771 (1994)

-
- 31 G. Braithwaite, N. L. Wattey, E. H. C. Parker, T. E. Whall, G. Brunthaler and G. Bauer, *Hot hole energy relaxation in Si/Si_{0.8}Ge_{0.2} two dimensional hole gases*, Journal of Applied Physics **81** (10) 6853-6856 (1997)
- 32 S. Agan, O. A. Mironov, E. H. C. Parker, T. E. Whall, C. P. Parry, V. Yu. Kashirin, Yu. F. Komnik, Vit. B. Krasovitsky and C. J. Emeleus, *Low-temperature electron transport in Si with an MBE-grown Sb δ layer*, Physical Review B **63** 075402 (2001)
- 33 M. J. Kearney, A. I. Horrell and V. M. Dwyer, *The transport-time to state-lifetime ratio in semiconductor quantum-well alloys: a multiple scattering analysis*, Semiconductor Science and Technology **15** 24-31 (2000)
- 34 K. Ismail, M. Arafa, K. L. Saenger, J. O. Chu and B. S. Meyerson, *Extremely high electron mobility in Si/SiGe modulation-doped heterostructures*, Applied Physics Letters **66** (9) 1077-1079 (1995)
- 35 F. Stern and S. E. Laux, *Charge transfer and low-temperature electron mobility in a strained Si layer in relaxed Si_{1-x}Ge_x*, Applied Physics Letters **61** (9) 1110-1112 (1992)
- 36 J. J. Harris, K. J. Lee, T. Wang, S. Sakai, Z. Bougrioua, I. Moerman, E. J. Thrush, J. B. Webb, H. Tang, T. Martin, D. K. Maude and J-C Portal, *Relationship between classical and quantum lifetimes in AlGaIn/GaN heterostructures*, Semiconductor Science and Technology **16** 402-405 (2001)
- 37 L. B. Rigal, D. K. Maude, M. Potemski, J. C. Portal, L. Eaves, Z. R. Wasilewski, G. Hill and M. A. Pate, *Phase Diagram for the Breakdown of the Quantum Hall Effect*, Physical Review Letters **82** (6) 1249-1252 (1999)
- 38 J. J. Harris, K. J. Lee, D. K. Maude, J-C Portal, T. Wang and S. Sakai, *Phase diagram for the quantum Hall effect in a high-mobility AlGaIn/GaN heterostructure*, Journal of Physics: Condensed Matter **13** L175-L181 (2001)
- 39 G. Nachtwei, *Breakdown of the quantum Hall effect*, Physica E **4** 79-101 (1999)
- 40 S. Komiyama and Y. Kawaguchi, *Heat instability of quantum Hall conductors*, Physical Review B **61** (3) 2014-2027 (2000)
- 41 W. Desrat, D. K. Maude, L. B. Rigal, M. Potemski, J. C. Portal, L. Eaves, M. Henini, Z. R. Wasilewski, A. Toropov, G. Hill and M. A. Pate, *Low-frequency impedance of quantized Hall conductors*, Physical Review B **62** (19) 12990-12996 (2000)
- 42 H. Iizuka, S. Kawaji and T. Okamoto, *Collapse of quantized Hall resistance and breakdown of dissipationless state in the integer quantum Hall effect: filling factor dependence*, Physica E **6** 132-135 (2000)
- 43 L. Eaves, *Quantum Hall effect breakdown steps: evidence for an instability induced by inter-Landau level scattering*, Physica B **298** 1-7 (2001)
- 44 Y. Morita, Y. Hatsugai, *Breakdown of the IQHE and the selection rule*, Physica B **298** 24-27

(2001)

45 K. Takashina, R. J. Nicholas, B. Kardynal, N. J. Mason, D. K. Maude, J. C. Portal, *Breakdown of the quantum Hall effect in an electron-hole system*, Physica B **298** 8-12 (2001)

46 G. Baccarani and P. Ostoja, *Electron Mobility Empirically Related to the Phosphorus Concentration in Silicon*, Solid State Electronics **18** (6) 579-580 (1975)